UNIVERSITÀ DEGLI STUDI DI PADOVA

Università degli Studi di Padova

Dipartimento dei Beni Culturali: Archeologia,
Storia dell'Arte, del Cinema e della Musica

Master Degree in
ARCHAEOLOGICAL SCIENCES

Curriculum in
APPLIED SCIENCES TO CULTURAL HERITAGE, MATERIALS, AND SITES

Experimental characterization of a historical F.C. Vogel photograph of Mons. Zinelli

Supervisor:
Prof. Gilberto Artioli
Co-supervisor:
Prof. Ivana Angelini

Master Candidate:

Mahsa Karimi

2070765

ACADEMIC YEAR 2025/2026

To the man who carried the deepest blue – my dearest Uncle:

Ali Mohammadian!

...به آبی ترین مردِ جهان، دایی جانم **علی محمّدیان!**

...and my dear sister ***Mahtab.***

...و خواهر عزیزم **مهتاب.**

Acknowledgments

First of all, I would like to express my deepest and most sincere gratitude to my supervisor, Professor Gilberto Artioli, for all his support in shaping and developing this project, for his careful and continuous feedback, and above all, for the trust he placed in me throughout this journey. I would also like to sincerely thank my co-supervisor, Professor Ivana Angelini, for all her advice, guidance, and valuable support.

I am also very grateful to Professor Alfonso Zoleo, Anna Piccolo, and Moari, who, despite all the responsibilities and difficulties of their own research, were always willing to help and support me. I learned a great deal from the three of you, from your patience, your support, and the knowledge you shared with me.

I would also like to thank my Mom, Daddy, my brother Mahyar, and my sister Mahtab, who have always encouraged and supported me throughout this journey. Without their love, support, and reassurance, this path would have been much harder to walk.

I would like to take this opportunity to give my warmest thanks to my friends:

Roshanak Ekrani and Elham Arianpour; you are many kilometres away from where I am standing today, writing these words, but distance never made me feel your presence or support any less. Even while carrying your own difficulties, you always believed in me and in my ability to succeed. Without the two of you, and without the hope you kept sending me from afar, I probably would not have been able to make it through even half of this journey.

Atiyeh Paziyar, Monireh Azad, and Elaheh Zeighami; this journey was hard. It had many dark moments, many disappointments, wounds, and periods of confusion that sometimes felt heavier than the happy moments. But you were there, exactly where you needed to be. It is probably impossible to describe in just a few lines all those long nights when, if we had not had each other, we would not have known with what feeling we would reach the morning. But we were lucky to have one another. Thank you for every moment when I thought I could not go any further, and you took my hand and, like sisters, reminded me that brighter and better days would come — and they did. Without you, this journey might have stopped at its very first uphill steps.

Arash Ershadi; I learned so much from you that I cannot simply forget your presence. Your kindness, your smile, and the joy you brought with you often worked like a catalyst on difficult days, making the path feel lighter and helping me move forward with a smile and a better feeling.

And finally, I want to thank **myself**. For all those nights that were hard, painful, and dark, but I did not let myself drown in their darkness. For all those moments when I was so close to reaching the things I wanted, but lost them, and still, wounded and exhausted, I stood up again, kept going, kept hoping, and finally succeeded. I am grateful to myself for pushing aside the disappointments, the things that did not happen, and the things that were not meant for me, and for finally finding peace in a place, and with people, where I truly felt safe and genuinely wanted — people like Atiyeh, Monireh, and Elaheh

And the last words are for you, dear uncle. You are so far away that I can no longer see you or hear your voice. But remember this: wherever there is a story about how hard I tried, you were there. You were part of it. In fact, it was because of you that so many things moved forward and ended up exactly where they were meant to be. Thank you for everything, and for **"**being a hero**"** — perhaps the greatest legacy you could have left behind for us.

I will do everything I can to be like you, so that from wherever you are watching me, you can be happy, clap for me, and open your arms for that strong, tight hug that I will never get to have again — and be proud of me.

Abstract | Sommario

This study investigates a historical photograph dating from approximately 1850–1855, produced by the German photographer and lithographer Friedrich Carl Vogel and depicting the Venetian bishop Federico Maria Zinelli. The photograph consists of three layers and presents extensive yellowing, severe fading, and foxing. These deterioration phenomena complicated both the analytical investigation and the identification of the original photographic process.

The aim of this research was to characterize the materials and stratigraphy of the photograph and to determine the photographic technique used for its production. A multi-analytical approach was therefore employed, combining optical microscopy, confocal microscopy, ATR-FTIR, micro-FTIR, and X-ray fluorescence (XRF). These techniques were used to investigate the surface morphology, layer structure, constituent materials, and the presence of organic binders and associated elements.

The interpretation of the analytical results was integrated with historical information, the observed deterioration patterns, and comparisons with previous studies on nineteenth-century photographic processes. Three possible techniques were considered: salt printing, albumen printing, and gelatin printing. The combined evidence, including the identification of protein-based binders, the stratigraphic structure, and the elemental and morphological characteristics of the photograph, suggests that the object was most likely produced using a single-coated albumen printing process.

A definitive identification would require further analytical techniques involving direct sampling. However, because the photographic layer occupies only a limited portion of the object, even minimal sampling could result in irreversible damage. The study therefore highlights both the potential and the limitations of a primarily non-invasive and minimally invasive analytical approach for the characterization of fragile historical photographs.

Questo studio esamina una fotografia storica databile approssimativamente tra il 1850 e il 1855, realizzata dal fotografo e litografo tedesco Friedrich Carl Vogel e raffigurante il vescovo veneziano Federico Maria Zinelli. La fotografia è costituita da tre strati e presenta un esteso ingiallimento, un forte sbiadimento e fenomeni di foxing. Questi fenomeni di degrado hanno reso più complessi sia il processo di analisi sia l'identificazione del procedimento fotografico originale.

L'obiettivo di questa ricerca era caratterizzare i materiali e la struttura stratigrafica della fotografia e determinare la tecnica fotografica utilizzata per la sua realizzazione. A tale scopo è stato adottato un approccio multi-analitico che ha combinato microscopia ottica, microscopia confocale, ATR-FTIR, micro-FTIR e fluorescenza a raggi X (XRF). Queste tecniche sono state impiegate per analizzare la morfologia superficiale, la struttura degli strati, i materiali costitutivi e la presenza di leganti organici e degli elementi ad essi associati.

L'interpretazione dei risultati analitici è stata integrata con le informazioni storiche, i fenomeni di degrado osservati e il confronto con studi precedenti relativi ai procedimenti fotografici del XIX secolo. Sono state prese in considerazione tre possibili tecniche: la stampa salata, la stampa all'albumina e la stampa alla gelatina. L'insieme delle evidenze, tra cui l'identificazione di leganti di natura proteica, la struttura stratigrafica e le caratteristiche elementari e morfologiche della fotografia, suggerisce che l'opera sia stata molto probabilmente realizzata mediante un procedimento di stampa all'albumina a singolo strato.

Per ottenere un'identificazione definitiva sarebbero necessarie ulteriori tecniche analitiche che richiedono un campionamento diretto. Tuttavia, poiché lo strato fotografico costituisce solo una parte limitata dell'intero oggetto, anche un campionamento minimo potrebbe causare danni irreversibili. Lo studio mette quindi in evidenza sia le potenzialità sia i limiti di un approccio analitico prevalentemente non invasivo e minimamente invasivo per la caratterizzazione di fotografie storiche fragili.

Introduction

In a world saturated with images, the photograph has become almost invisible. Photographs are among the most common objects we encounter and exchange every day. Yet their very familiarity often prevents us from recognizing the deeper complexities and questions that lie beneath their ordinary presence (Clarke 1997). During the nineteenth and twentieth centuries, a photograph was generally defined as a visible and permanent image formed on some type of support that had been produced by the effect of visible or invisible radiation on a light-sensitive surface (Lavedrine 2009). However, The 21st century represents a major transition in the history of photography. Traditional photography is gradually being replaced by digital imaging, changing the way photographs are created, viewed, and preserved. Although photographs today are more often viewed on screens than printed on paper, this shift has not decreased their significance. In fact, photographic collections have become an important part of collective memory and cultural heritage. As a result, the preservation and protection of photographs have become essential for contemporary society (Lavedrine 2003).

Around the late 1840s, people were still excited about the new invention of photography when a big problem started to show up. While daguerreotypes stayed in good shape, many paper photographs began to fade or get stained. Some almost disappeared completely. People complained about spots, yellowing, and uneven colors. It became clear that something in the way these photos were made or stored was causing them to get ruined quickly — and this made some people wonder if photography on paper could really be trusted at all. Although progress had been made in establishing the causes of print fading, it was still questionable if any print would persist beyond a few years. The variety of base papers, binder materials, and processing chemicals used at the period made it difficult to determine the exact causes of fading (Reilly 1980). Hence, the identification of structural elements and materials is a crucial and foundational step in a key phase to create suitable methods for restoration, preservation, and serious damage avoidance. It identifies the best method for preserving photographs to ensure the most suitable conservation or preservation approach (Oravec et al. 2019).

The goal of this study is to determine the materials and photographic technique used to produce an image from the *Archivio Fotografico del Seminario Vescovile di Treviso*, taken between 1851 and 1855 by Friedrich Carl Vogel, a German photographer and lithographer from Frankfurt, by integrating historical research with materials-science analysis. The study also aims to evaluate the photograph's current state of preservation in order to support future conservation work.

1. Historical and Technical background

1.1 the invention of photography

Although most authors believe that the development of photography resulted from the experiments of the German physicist Johann Heinrich Schulze around 1727, who discovered the sensitivity of silver nitrate to the light rather than to heat (Peres 2007), it was Thomas Wedgwood (British, 1771–1805) who produced the first photograms at the end of the eighteenth century and also made effort to take first images by a *camera obscura*[1] (Stulik and Kaplan 2013). A photogram is an image made without a camera by placing two or three-dimentional objects directly on photographic paper or film and exposing them to light (International center of photography 1984). Wedgwood and his collegue Sir Humphrey Davy made their photograms on paper and white leather coated with silver nitrate, but they could not fix and prevent them from fading (Peres 2007). A French man named Joseph Nicéphore Niépce (French, 1765_1833) was the first person to make a permanent photograph. In 1826, he took a picture on metal from the window of his attic (Fig. 1). The photo needed about eight hours of exposure to be created (Clarke 1997). He gave up using silver chloride in his expriments, hence, replaced a light-sensitive solution of Bitumen of Judea _an asphalt compound_ to create photographic images. Niépce chose the term "heliography" to describe his photographic process. The word comes from two Greek roots: *helio*, meaning "sun," and *graphien*, meaning "to write" or "to draw" (International center of photography 1984).

[1] The *camera obscura* (meaning "dark room") is an optical device that projects an image of the outside world onto a surface inside a dark space, allowing it to be observed and traced. It played an important role in the study of light and perspective and is considered one of the precursors to the development of photography. History of Science Museum, University of Oxford, "Camera Obscura". accessed August 25, 2026, https://www.hsm.ox.ac.uk/camera-obscura

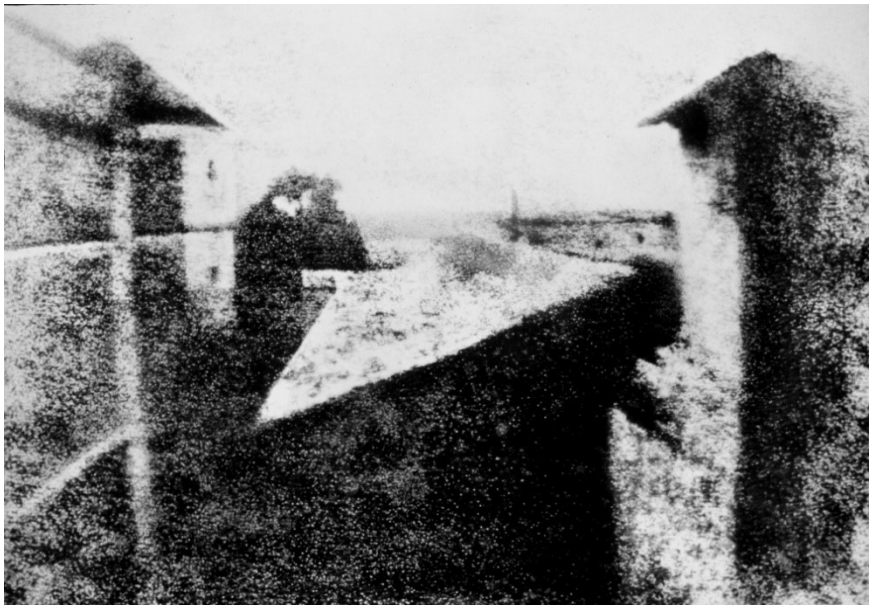

Fig. 1. Joseph Nicéphore Niépce, View from His Window at Le Gras. Heliograph on pewter. 1826

Source: Brown, Barbara. “The First Photograph.” *WAAC Newsletter* 26, no. 3 (2002).

In December 1834, Louis Jacques Mandé Daguerre (French, 1787–1851) discovered that when a silver-coated plate was exposed to light and treated with mercury vapor, a pale silver-mercury layer appeared and created a very detailed image. This method also reduced the exposure time to about 20 minutes in bright sunlight. He could fix his images by a chemical called sodium hyposulphite, or "hypo," discovered by an astronomer and chemist Sir John Herschel (British, 1792–1871), and prevent them from fading. On January 7, 1839 Daguerre‘s photography process presented to the Académie des sciences in Paris and he called it *Daguerreotype* (Hirsch 2024). The announcement of the Daguerreotype process in January 1839 inspired William Henry Fox Talbot (British, 1800–1877) to advance his photographic research, resulting in the salt print negative-positive process on paper (Stulik and Kaplan 2013).

1.2 Salt print

During the history of photography the word “salt” refers to sodium chloride was the first halide used together with silver (Peres 2007). Hence, the term “salt paper process” refers to any method that prepares salts of silvers such as chlorides, bromides, and iodides directly on a paper (not in a coating of Gelatin)(International center of photography 1984).

William Henry Fox Talbot began his expriments with silver chloride in 1834, but in 1841 he changed his formula to use silver iodic that was more sensitive, so he could significantly decreased the exposure time (Peres 2007).with only four important chemicals such as silver nitrate and potassium iodide (to make silver iodide), acetic acid and gallic acid he made first paper negative. During the first step he called “iodizing”, silver nitrate and potassium iodid were brushed over a fine writing paper and was allowed to dry. The result of first step needed more sensitivity to light, hence in second stage, Talbot excited the iodized paper by treating its surface with silver nitrate, acetic acid and gallic acid. After exposure, an unseen latent imaged formed. With using gallic acid to develop the invisible image and fixing it with hypo, Talbot invented the Calotype or Talbotype process (Taylor and Ware 2015). Although these in-camera images were negatives, with the bright areas of the scene recorded as dark and the shadows as light, Talbot’s aim was to obtain direct positive photographs (Hirsch 2024). Talbot solved the problem of tonal reversal by reprinting the paper negative in direct contact with an unexposed sheet of plain silver chloride paper under sunlight. Hence, the reversed tones of the negative were reversed once again, producing a positive image of color ranging from deep orange to cool brown called Salt paper print (International center of photography 1984). Because of these developments, Talbot is usually considered to be the inventor of paper_bases photography (Stulik and Kaplan 2013).

1.3 Albumen process

1.3.1 What is albumen?

Albumen is a clear, slightly yellowish liquid made of animal or plant proteins. In traditional photographic processes, it was most commonly obtained from fresh hen's eggs (International center of photography 1984).

1.3.2 The invention of Albumen print

In 1847, Abel Niépce de Saint-Victor introduced a new glass-negative process called the niépceotype. It used egg albumen to bind the light-sensitive silver iodide to glass plates. Although the process produced high-quality results, both exposure and development took longer than with the calotype (International center of photography 1984). On the other hand, At the end of 1840s a talented, technical photographer named Louis Desire Blanquart-Evrard (French, 1802-1872) invented albumen paper and presented his discovery to the French Academy of Sciences on 1850 (Reilly 1980). He added an equal amount of albumen to chloride solution (sodium or ammonium) (1:1 ratio) to prevent the image from penetrating too deeply into the paper fibers and make a final slightly glossy print (International center of photography 1984). To sensitize the paper he used a concentrated silver nitrate solution, then dried and exposed it to daylight (Reilly 1980). In summary, the production of Albumen paper has nine steps (Ricci Bloxham and Kazarian 2007):

1- Separate the egg whites from the yolks
2- Beat the egg whites with ammonium chloride and/or sodium chloride (NH_4Cl, NaCl) until a foam is formed
3- Leave the foam to settle
4- Strain the liquid mixture
5- Age the mixture
6- Float the sheet support on the mixture
7- Hang the coated sheet to dry.
8- Leave the coated sheet to harden and cure
9- Placing its coated surface face down on a silver nitrate ($AgNO_3$) solution to sensitise.

Albumen paper was very similar to plain salted paper, but egg white was used as a binder to close pores of paper and keep the light-sensitive materials on its surface (Fig. 2).This produced sharper, stronger, and more detailed prints with better contrast (Reilly 1980). Although the majority of Albumen photographs had toning[2], some of them, specially tested ones, were left untoned. The color of albumen photographs varies depending on the quality of darkroom processing and their condition over time. Their tones can range from very light brown to brown, reddish brown and deep violet-black.The level of glossiness of albumen prints continuously evolved from the early development of this technique until after 1870; it was influenced by public preference for photographs with glossy, semi-glossy, or matte surfaces (Stulik and Kaplan 2013).

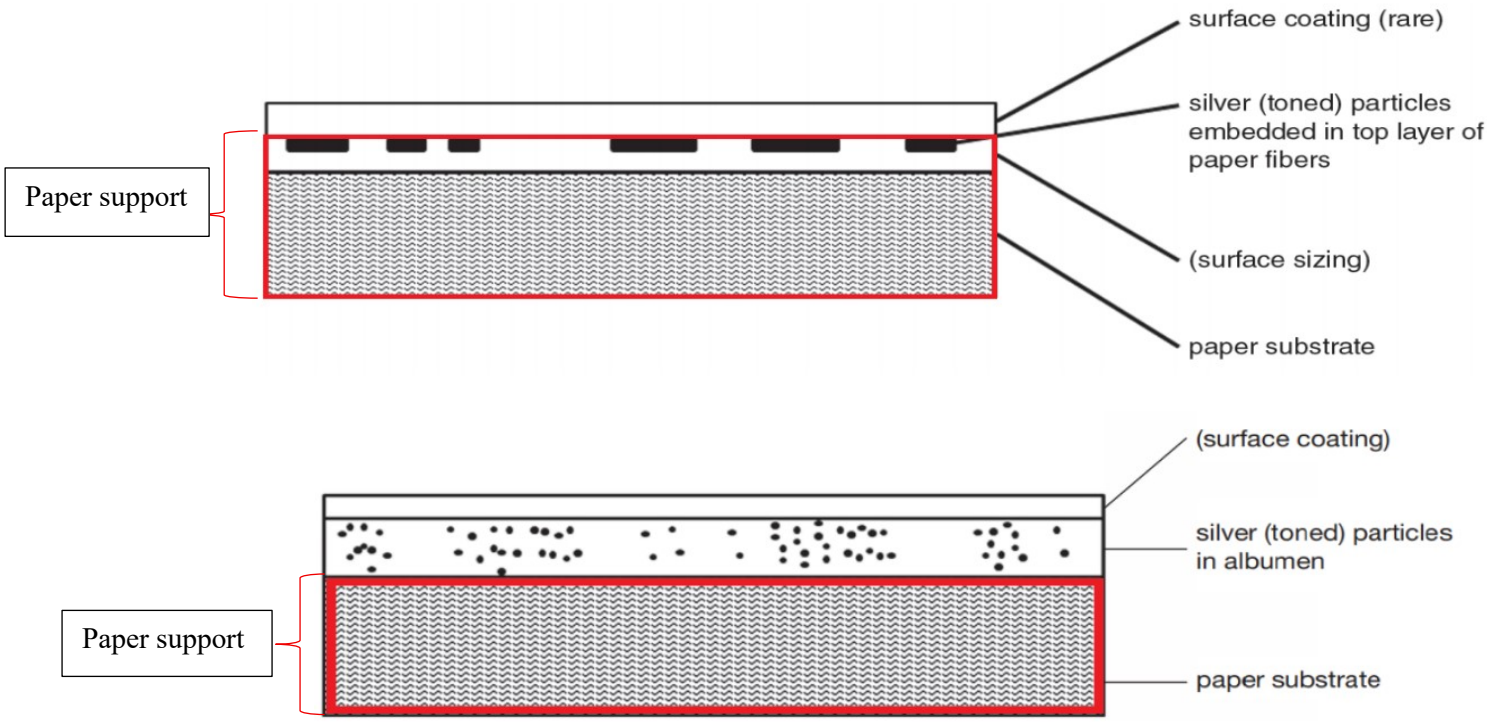

Fig. 2. Schematic cross section of salt print and albumen print photograph. A) in salt print photograph, reduced silver particles were deposited on the surface of the paper and within the spaces between its individual fibers. B) in Albumen print photograph, reduced silver particles are embedded in a seprate albumen layer on top of the support paper (Stulik and Kaplan 2013).

[2] Toning is a chemical process used in monochrome photography to alter the colour of photographic prints. Camera-wiki, "Toning," accessed August 25, 2026, https://camera-wiki.org/wiki/Toning.

2 Sample and Instruments

2.1 Sample, photographer, and subject

The sample under investigation is a photograph from the *Archivio fotografico del Seminario vescovile di Treviso,* taken about 1850-1855 by Friedrich Carl Vogel, a German photographer and lithographer from Frankfurt working in Venice at the time (Fig 1). It consists of three layers: the support paper, the brown paper, and the photo card. the first and second sections are rectangular, with dimensions of 217 mm × 190 mm, and 132 mm × 126 mm respectively; and the third layer is circular, with a radius of 120 mm. The first two sections have a matte face, while the circular photo part shows some gloss and reflection when held under light. The thickness of brown support and photocard layer is respectively around 130 µm and 70 µm. Most old photographs were mounted on paper substrate, specially albumen photographic papers because they were too thin to stay strongly with no tendency to curl inside (Stulik and Kaplan 2013).

The photographic archive of the Episcopal Seminary of Treviso (*Archivio fotografico del Seminario vescovile di Treviso*) houses over 130,000 items, including prints, negatives, slides, and early photographic equipment, spanning. from the mid-19th century to the early 2000s. It also holds more than 40,000 postcards, films, and audio recordings. The collection covers religious life, historical events, artworks, and city views, and includes major private collections from notable clergy. Its oldest section features works by leading Italian and international photographers of the 19th and 20th centuries. In addition, the archiving of the materials has been organized according to standards and best practices for long-term conservation, and more recently a restoration and digitalization have been started for the most vulnerable materials (Seminario Vescovile della Diocesi di Treviso 2020).

Friedric Carl Vogel was an active portrait photographer in the mid-19th century. In May 1850, he moved to Milan, where he established a studio for Talbotype portraits. Previously, he had worked in Frankfurt, serving high-status clients. His sitters included members of European nobility, such as the King of Bavaria, the heir to the Grand Duke of Russia, and the Prince of Prussia. He

collaborated closely with his wife, who helped arrange the poses. Vogel maintained a respectful and enthusiastic correspondence with William Henry Fox Talbot, expressing admiration for his invention and professional interest in his photographic approach (Vogel 1851).

The subject of picture is Federico Maria Zinelli was born in Venice on June 23, 1805, into a recently ennobled family. He studied in Padua and entered the seminary in Venice in 1821, despite opposition from his parents. He was ordained in 1827 and spent more than twenty years teaching literature, philosophy, canon law, and theology. In 1839, he published *Biblioteca dell'ecclesiastico*, a practical guide to essential books for priests. Zinelli also wrote on religion, science, and philosophy, and worked with several prominent Venetian intellectuals. During the 1848–49 revolutions, he supported the Venetian republic but criticized policies that weakened the Church. Later, he opposed the unification of Italy and defended the Pope's political role. In 1861, he was appointed Bishop of Treviso. He supported the doctrine of papal infallibility during the First Vatican Council and died in Treviso on 24 November 1879 (Baruzzo 2020).

2.2 Instruments

The three-layer photo was examined with a combination of microscopic and spectroscopic tecniques such as optical microscopy (OM), confocal laser scanning microscopy (CLSM), Fourier transform Infra-red spectroscopy in attenuated total reflectance mode (ATR-FTIR), and portable X-ray fluorescence spectroscopy (pXRF). Each one of these techniques has a specific function to identify chemical and microstructural characteristics of the paper and the materials used to make the photo. The adopted techniques are all non-invasive, thus including no damage to this unique item. Since the sample dates back over 170 years and is extremely fragile due to its paper-based nature, all of the applied techniques have been carefully selected to ensure the complete preservation of the photograph, avoiding any form of damage or alteration.

2.2.1 Optical Microscopy

Optical microscopy employes a polarized light microscope and it is widely applicable to all solid samples. If applied in the reflected-light mode, the photograph can be directly imaged with no damage or manipulation. Modern microscopes can readily be equipped with CCD cameras to record and analyze digital pictures (Artioli 2010). Using a Nikon ME 600 microscope under reflected light in different magnification scales between 5x and 20x in different numerical apertures without applying cross-polarized (XPL) plus a digital Canon 600D EOS camera and EOS Utility software show details of each three layers, illustrating the fiber arrangements and the paper foxing at different magnifications. All studies related to Optical Microscopy took place at the Department of Geoscience at the University of Padova (Fig. 3).

Fig. 3. The polarized microscope *Nikon Eclipse ME600* with five objectives (5x, 10x, 20x, 50x and 100x) equipped with a Canon *EOS 600D camera* in the Geoscience department of University of Padova.

2.2.2 Confocal Microscopy

The primary functions of a confocal microscope are to produce a point source of light and reject out-of-focus light. This provides the ability to image deep into tissues with high resolution, and the ability to capture thin layers of the sample at different depths (like slicing it optically without cutting)(Elliott 2020). A laser beam scans the sample point by point to build at the same time high-resolution optical and 3D laser interferometric images of the scanned surfaces (Nieto-Villena et al. 2019). The reflected light from the measured surface passes through a pinhole aperture, allowing changes in surface elevation to be recorded. A series of focal slices acquired at different depths are then combined to reconstruct a three-dimensional digital map of the surface (Stemp et al. 2017). By being equipped with focus stacking, this technique enables the study of surface morphology (Nieto-Villena et al. 2019). Olympus LEXT OLS 4000 3D Laser Measuring Microscope in the Geoscience department of Padua University (courtesy of the CIRCe Centre) is supplied with 5x 10x 20x 50x and 100x lenses and with the stitching mode the associated software allows to create a mosaic image composed of high magnification single frames (Pellegrina 2024).

Fig. 4. *Olympus LEXT OLS 4000 3D* confocal laser scanning microscope in the Geoscience department of Padua University, courtesy of the CIRCe Centre.

2.2.3 ATR-FTIR

FTIR is a vibrational spectroscopy fit to evaluate the molecular components, especially organics (Derrick Stulik and Landry 2000). The mid-infrared (mid-IR) region is the most important part of the infrared spectrum for identifying organic materials commonly found in photographs, such as binders in the image layer, the image support (paper or polymer), and different coatings or varnishes used to protect or alter the appearance of photographic images (Artioli 2010). ATR-FTIR is especially suitable for non-invasive analysis because it allows the investigation of material surfaces without modifying or damaging the sample (Taati 2024). The infrared beam enters the ATR crystal and, when the angle of incidence is higher than the critical angle, it is totally reflected at the contact surface between the crystal and the sample. This reflection creates an evanescent wave penetrates a few micrometres into the sample. The evanescent wave interacts with the sample, and part of the infrared energy is absorbed depending on its composition and morphology. As a result, the reflected beam reaching the detector has a lower intensity (Kaur et al. 2021) (Fig. 5). ATR-FTIR spectra were recorded using a Bruker ALPHA II FTIR spectrometer (OPUS software) equipped with a diamond ATR crystal and a room-temperature DTGS detector. For each sample, 264 scans were averaged and the range of spectra chosen between 4000 to 400 cm^{-1}. Background spectra were collected in air.

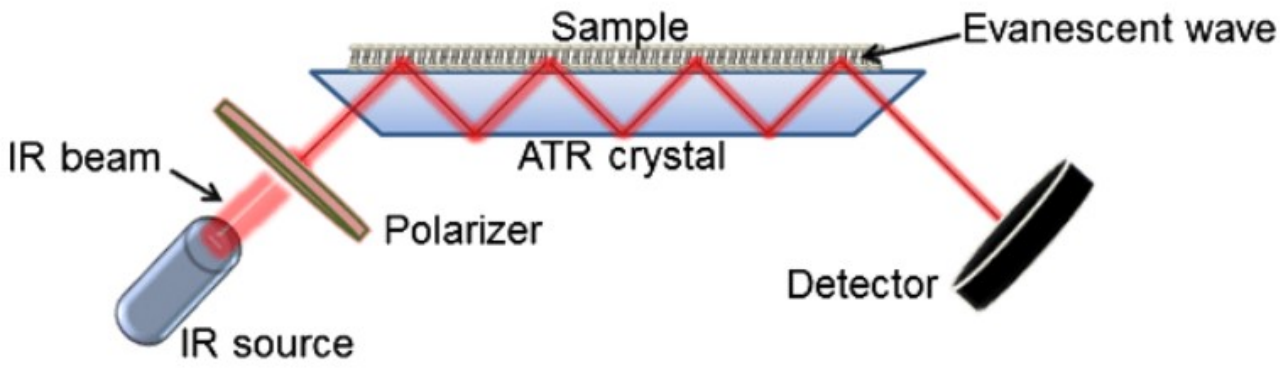

Fig. 5. Representation of ATR-FTIR system (Pellegrina 2024)

2.2.3.1 micro-FTIR

Micro-FTIR brings together FTIR spectroscopy and microscopy, making it possible to collect infrared spectra from very small, carefully selected areas. This allows for more precise analysis and can also be used to create FTIR maps showing how different materials are distributed across a sample. The micro-FTIR measurements were carried out in reflection mode using a Bruker Hyperion II FTIR microscope, shown in Figure 6. Spectra were recorded over the range of 4000 to 400 cm^{-1}, with 32 scans collected for each spectrum and a spectral resolution of 4 cm^{-1}. The data were collected and processed using Origin Pro software.

Fig. 6. Bruker Hyperion II FTIR microscope located at the University of Padova, Department of Geosciences

2.2.4 XRF

X-ray fluorescence spectrometry is based on the characteristic X-Ray emission from atoms stimulated by an external energetic Xray source. Using a portable probe (pXRF) it is possible to analyse in non invasive mode the surface of any material, and to measure the re-emitted signal using an energy dispersive analyser. X-rays can easily penetrate photographic paper to analyze the identification of the chemical elements inside the photo. All chemical elements above Na (Z>11). Elemental analyses were performed using a Bruker ELIO portable micro-XRF spectrometer equipped with XGLab electronics (CUBE preamplifier and DANTE digital pulse processor), courtesy of the CIBA Centre, UNIPD. The instrument is fitted with a rhodium (Rh) X-ray tube and a silicon drift detector (SDD) designed for high count rates and low electronic noise.

Measurements were carried out with the ELIO device (SN1257) in Head mode for point analyses under ambient air conditions. All analyses were conducted at the CEASC Centre, University of Padua. The X-ray beam spot size was about 1 mm, and precise positioning was ensured using dual laser alignment and an integrated microscope camera. Spectra were collected in manual mode, allowing the acquisition settings to be adjusted according to surface conditions and the expected elemental composition. A counting time of 120/240 s was used to improve the signal-to-noise ratio and facilitate trace-element detection while maintaining stable measurement conditions. The excitation voltage and current were set to 40/50 kV and 100 μA, respectively, to provide sufficient energy for the excitation of both light and heavy elements.

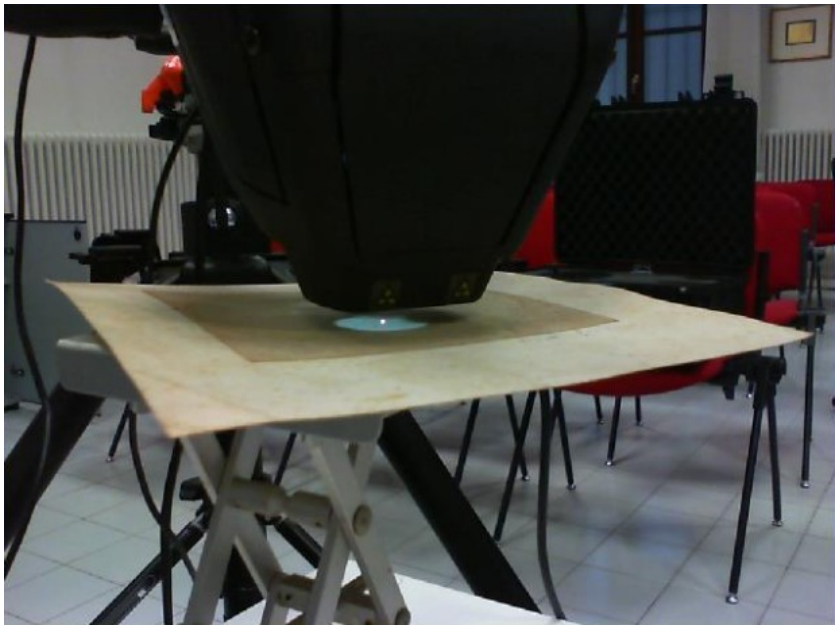

Fig.7. Portable X-ray fluorescence spectroscopy (p XRF) in the CEASC Centre of University of Padova, courtesy of the CIBA Centre.

3 Data and Results

3.1 Optical and Confocal microscopy

The microscopic examination and visual characteristics of the sample, together with techniques such as ATR-FTIR and XRF, can greatly assist in identifying the photographic process.

3.1.1 Foxing points

Using optical microscopy in different magnifications (5x, 10x, 20x) provided a precise observation of the surface of all three layers of photograph. According to visual charactristics, mentioned earlier, the surface of sample- in all 3 layers- is full of reddish to brownish spots as foxing and photo subject has significantly faded over time. Foxing is a form of chromatic alteration of old paper in different colors such as brownish, reddish, yellowish ,and blackish (Krstić et al. 2013). Foxing is present throughout the sample, not only in the form of isolated small circular spots, but also as irregular, elongated stains spreading across the surface. first group is usually round; some spots are reddish or brownish and well-delimited (Fig. 8), while others have black center and a yellowish halo around (Fig. 9) which according to previous experiments and studies, call them "bullseyes" (Figueira et al. 2020; Cain and Miller 1984). The second group of foxing, are lighter, irregular, and streaked across the surface even in some inches and named as "snowflake" (Fig. 10)(Ardelean and Melniciuc-Puică 2013; Cain and Miller 1984). Although foxing cause isn't completely clear, microorganisms and metallic impurities in paper play a major role in foxing formation (Krstić and Pavec 2013). Metal contamination may originate either during the papermaking process or from airborne dust. Previous studies on foxing spots in paper base materials detected Metals such as iron, tin, copper, copper–mercury or copper–zinc compounds in samples (Choi 2007). Subsequent studies also confirmed the presence of other elements, including potassium, oxygen, calcium, carbon and sulfur, in the foxed areas of the paper (Krstić and Pavec 2013).

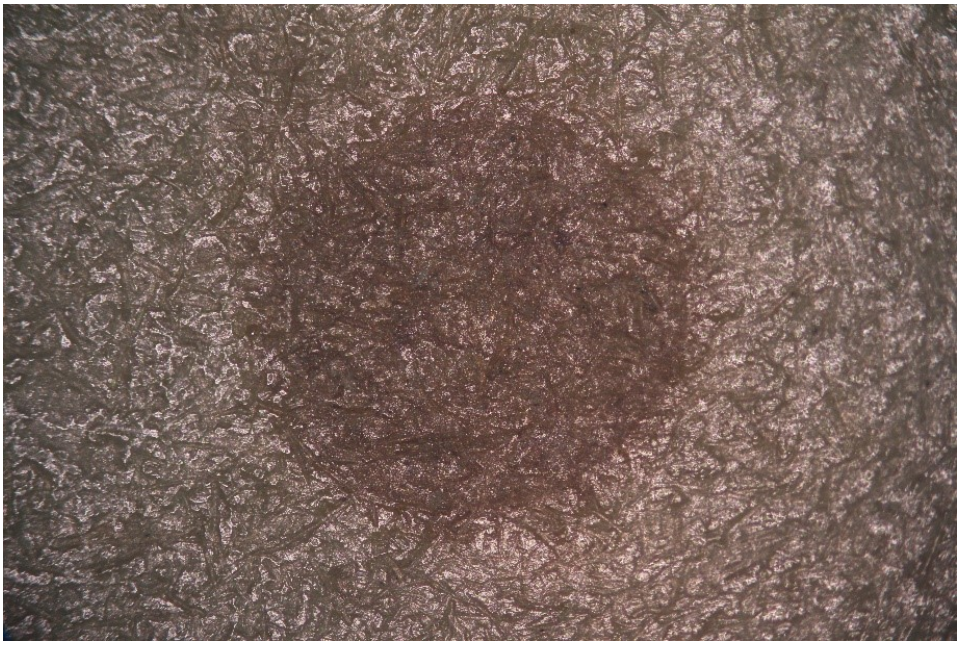

Fig.8.Optical Microscopy on the photo card, bullseyes foxing, reddish,well-round spot. in 5x magnification

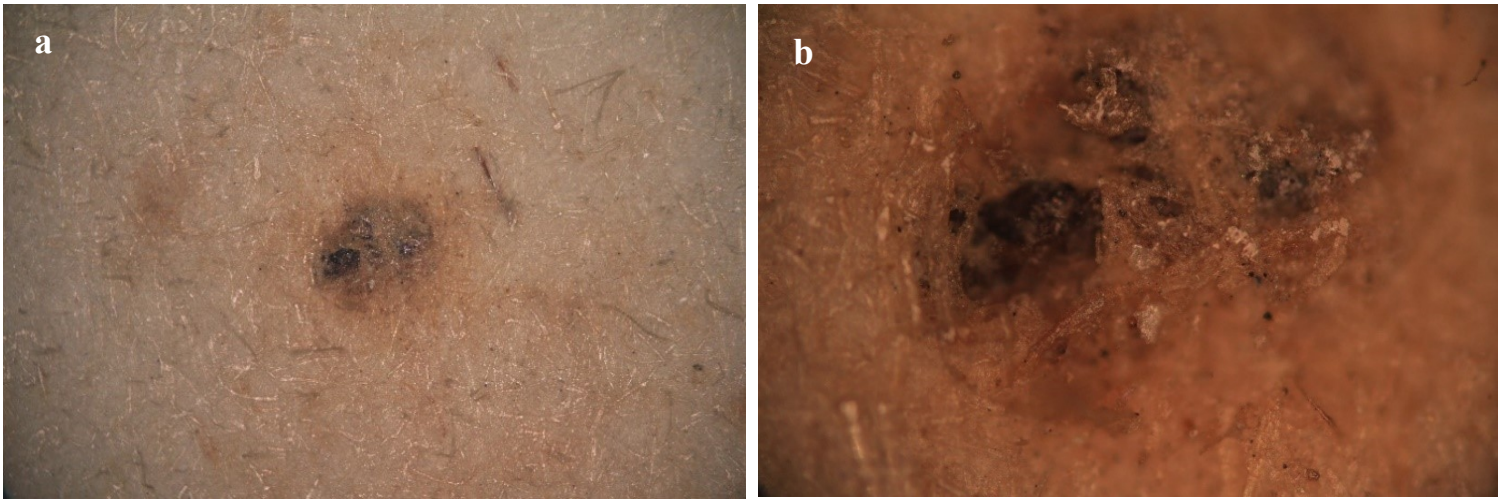

Fig.9. Optical Microscopy on the support layer. bullseyes foxing; with black center and light yellow centric rings arround. (a)5x, (b)20x

Fig. 10. Optical microscopy on the support layer, snowflake foxing; lighter with irregular shape. in 20x magnification

3.1.2 surface texture

A more in-depth examination to the sample surface reveals a clear difference between the surface layer of photo card and brown part. In comparison to salted paper prints which typically exhibit a rough or matt appearance, albumen prints are generally smooth and glossy (Fig.11) (Reilly 1980). Thanks to optical and confocal microscopy, the glossy surface of the sample could be observed, and its differences from the underlying surface (brown support) could be identified Fig.12 and 13.

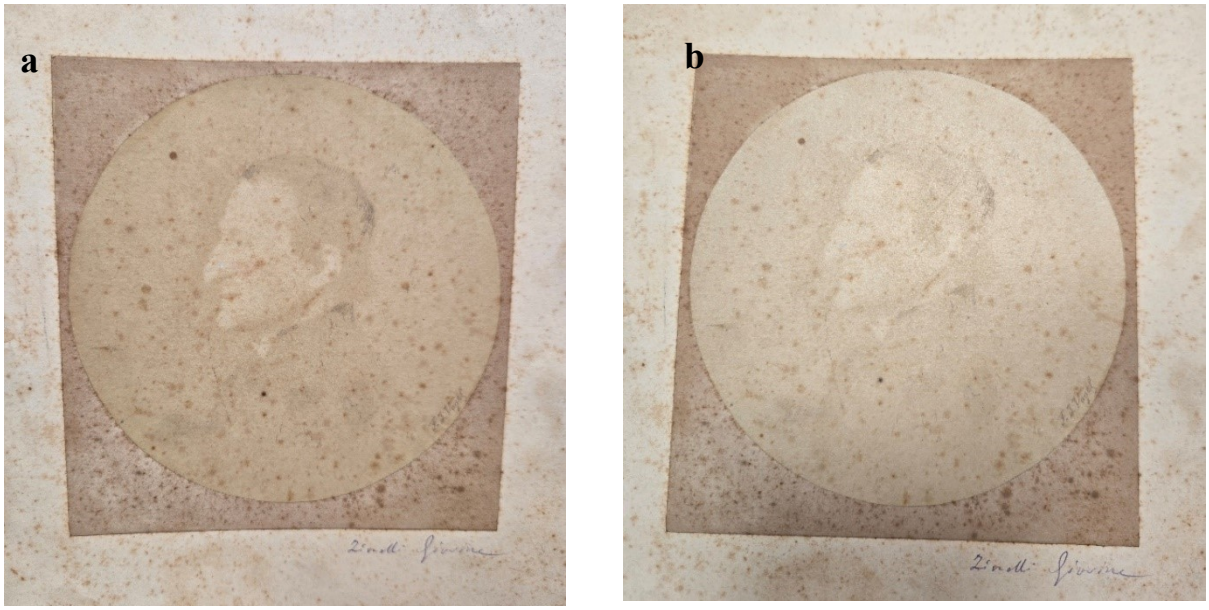

Fig. 11. Comparison of two photographic angles: (a) the sample photographed directly in front of the camera, with the camera parallel to the sample surface, showing no visible shine; (b) the sample photographed at a slight angle to the camera to reveal surface shine

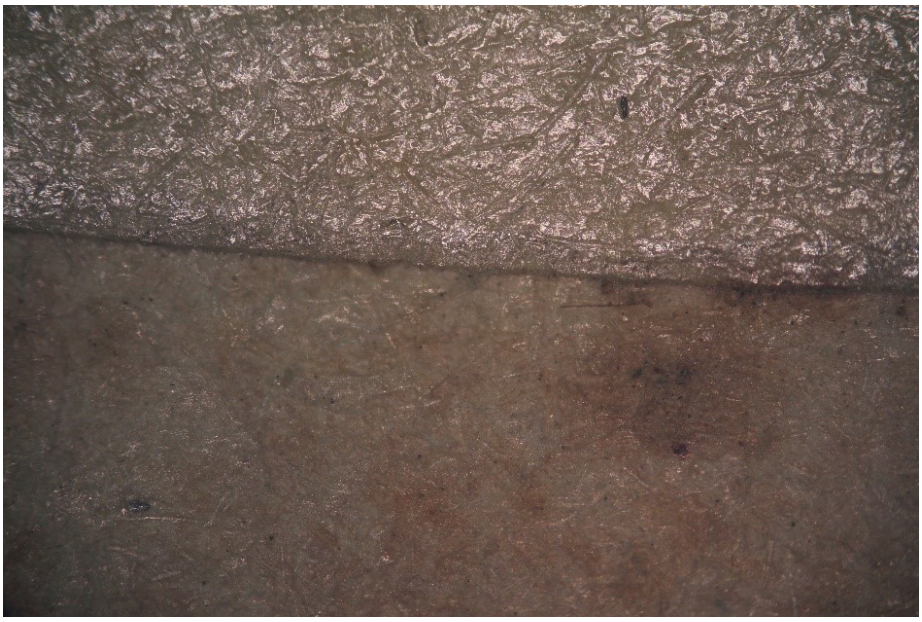

Fig. 12. The comparison between the surface of photo card and brown support shows the glossy surface of photo card. Optical Microscopy in 5x.

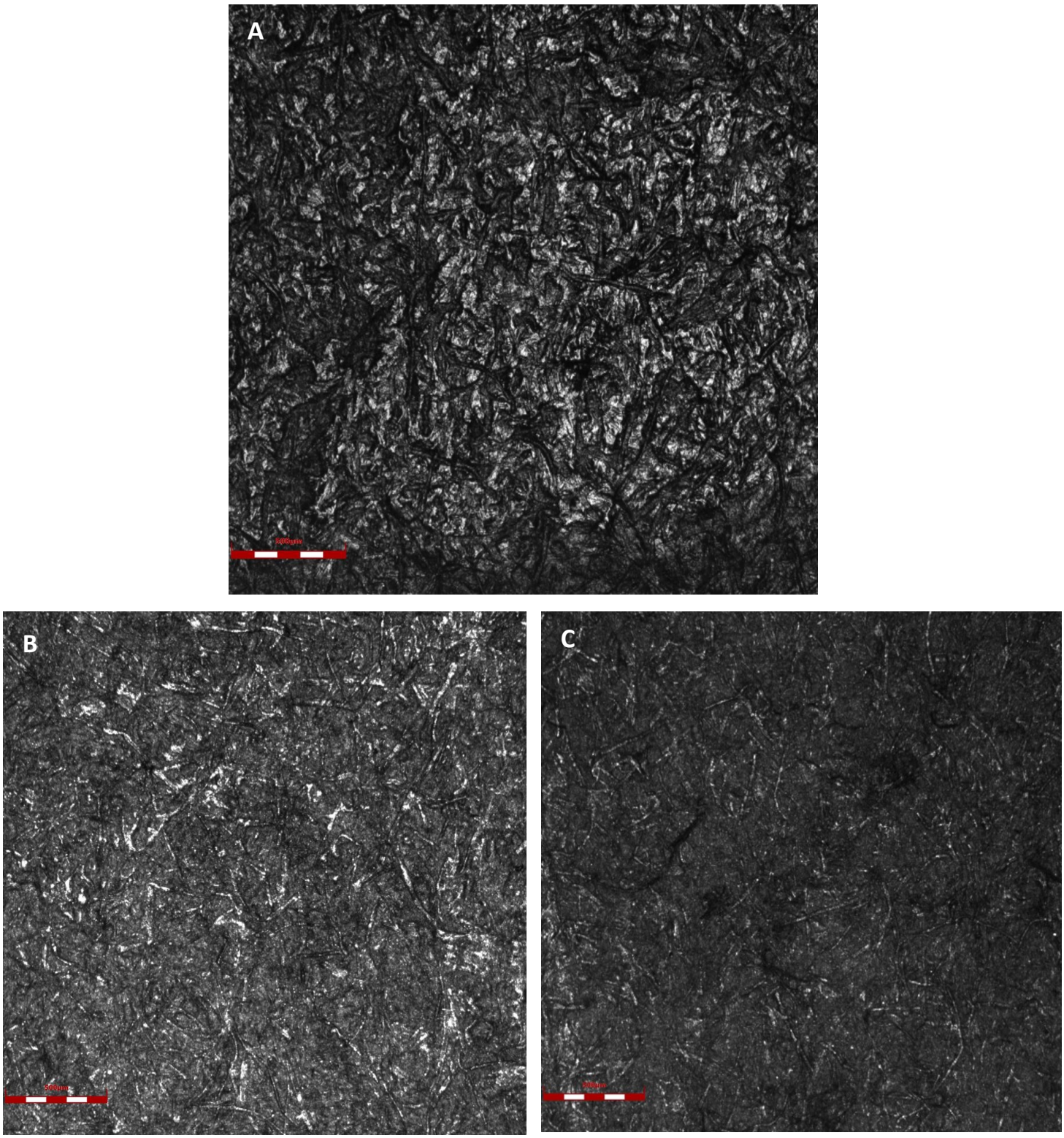

Fig. 13. Confocal microscopy: a comparison between the surface of photo card (a), brown support (b), and white support (c) shows the glossy surface of photo card. Scale bar 1s 500 μm

Although extensive cracking of the protein layer is a common characteristic used to identify albumen prints (Ricci et al. 2007), no network of crackes was observed on the surface of the photograph. Using a confocal microscope, images were acquired from three different layers of the sample at various magnifications to compare the structure and texture of the paper in each layer. In the resulting images (Fig. 14), the paper structure and individual fibers are clearly visible in both the brown and white support layers, as well as in the modern paper. In contrast, the photocard layer shows a smoother and more uniform surface, and the paper fibers are not as easily distinguished. This appearance may suggest that the fibers are immersed in a binder material or soaked with it, making the boundaries and individual structure of the fibers less clearly defined.

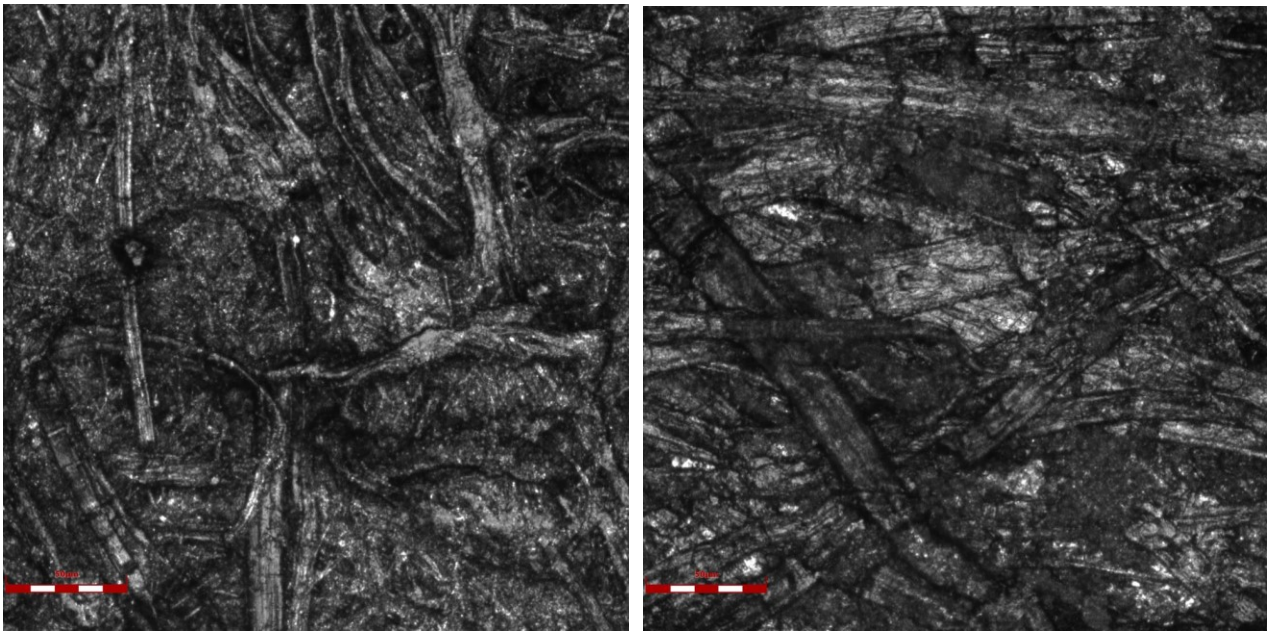

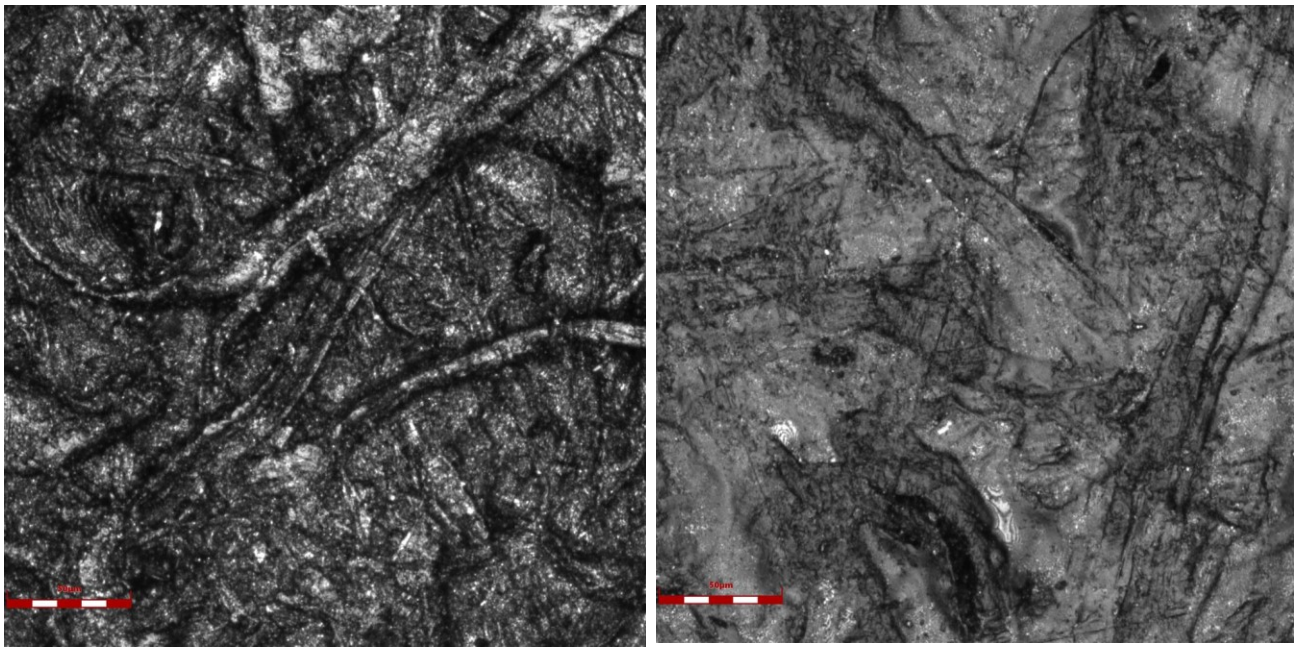

Fig.14. Confocal microscopy: a comparison of paper fibers between modern paper (a), white support (b), brown support (c), and photo card layer (d) shows the smooth surface of photo card's fibers soaked in a binder. Scale bar is 50 μm

Under microscopic magnification, the binder material could be seen pooling in the valleys and troughs between the paper fibers (Fig. 15a) . If this were simply a clear surface coating applied over a finished salted paper print, a more uniform distribution across the surface would generally be expected, and any pooled areas would tend to remain colorless regardless of the underlying image tone. In our sample, however, the binder was unevenly distributed (Fig. 15b), and the pooled areas were not completely colorless.The color and visibility of these pools can vary depending on the image tone. In mid-tone and darker areas, they are generally easier to detect because the binder appears more strongly colored, while in lighter or low-density areas they may appear as slightly yellowed or discolored patches against the white paper fibers. This relationship between the coloration of the pooled material and the image tone can indicate the presence of an albumen binder (Wagner et al. 2019). However, because the photograph has undergone extensive fading and much of its original tonal range has been lost, it was difficult to clearly evaluate this relationship in our sample. Small bubbles and holes were also visible in some areas of the binder layer, a feature that has also been reported in thin albumen coatings (Wagner et al. 2019) .

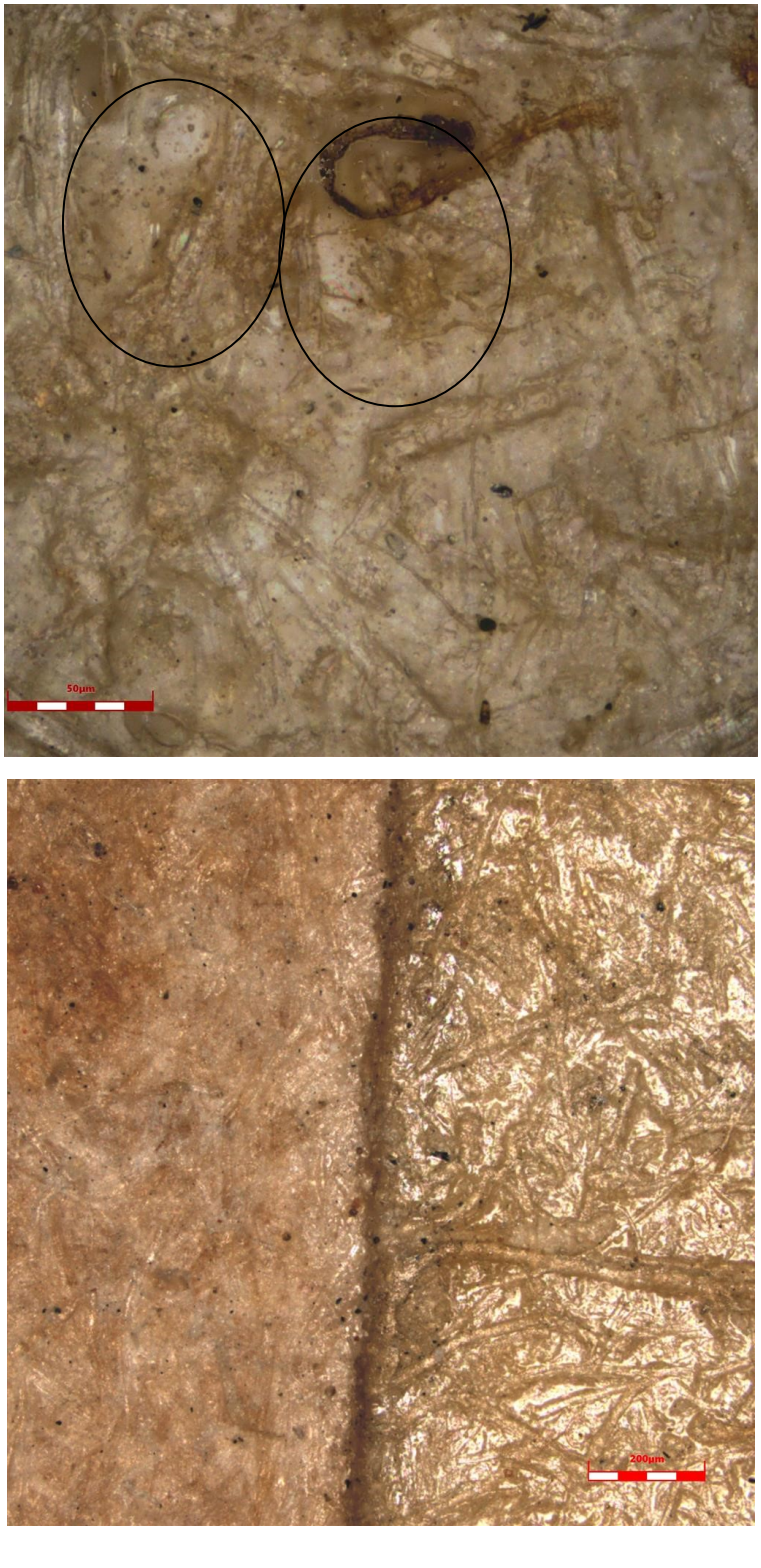

Fig. 15. (a) pooling of binder between fibers. Tiny Bubbles and small holes in the proteinous binder. Scale bar is 50 µm. (b) Non-uniform distribution of the binder over the surface of the photocard (right-hand layer), the cellulose fibers are clearly visible. Scale bar is 100 µm.

In the microscopic images of the white support layer, very small blue particles can be seen at different magnifications (Fig. 16). These particles are more numerous in the white support layer than in the brown support and the photocard layer. Previous studies have identified these particles as smalt, a pigment that was frequently added during the paper-making process. In the nineteenth century, pigments such as smalt or ultramarine were added to paper pulp during production to reduce the visible effect of the paper's natural yellowing (Barro et al. 2020).

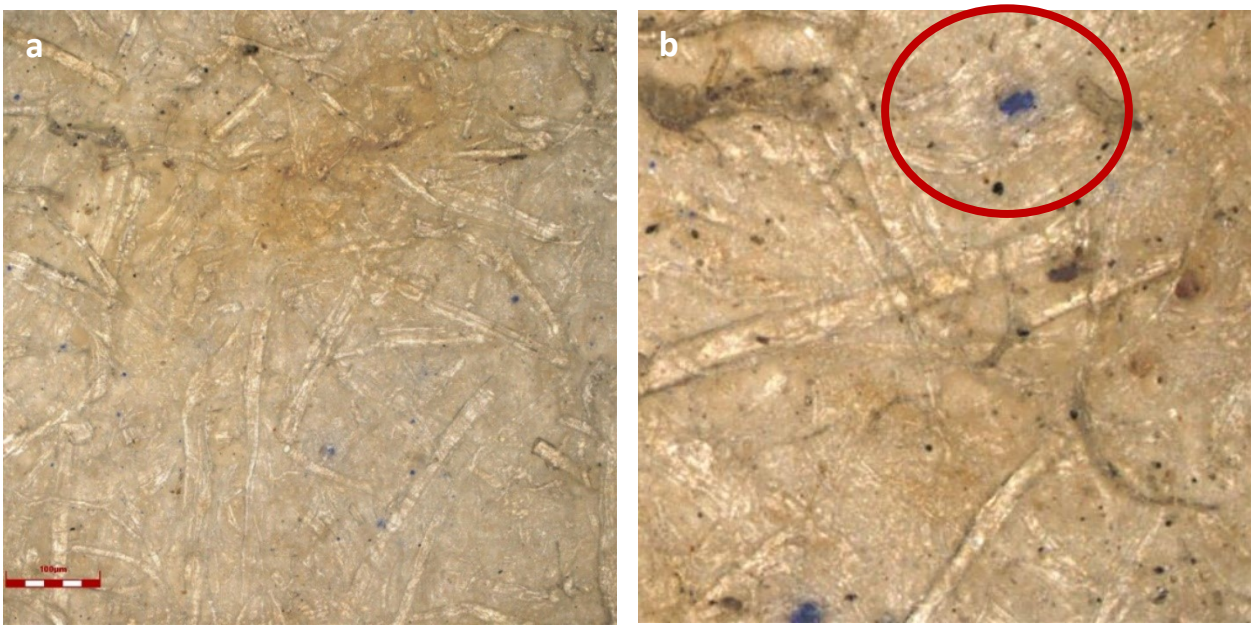

Fig. 16. (a) Tiny blue smalt particles in white support layer in 100 µm scale bar. (b) Cropped, magnified image of an angular, irregularly shaped smalt particle

At low magnification, these particles may appear simply as tiny impurities, but at higher magnification and under good lighting, their bright blue color becomes clearly visible (Stulik and Kaplan 2013). Smalt is a potassium-based cobalt glass that contains cobalt, potassium, silicon, and varying amounts of other elements, most commonly arsenic, nickel, and bismuth. Smalt particles usually appear as small, irregular glass-like fragments with sharp, angular edges and a characteristic conchoidal fracture under microscope (Barro et al. 2020).

As shown in Figure 16, parts of the subject's hair and the collar of his clothes were retouched. In the confocal microscope images, black particles, possibly related to graphite, can be clearly observed in the retouched areas. According to previous studies, many historical albumen portraits were retouched to correct imperfections caused by the negative or by the printing and processing stages. Retouching could also be used to emphasize or reduce certain details in the sitter or the background. In many cases, the materials used for retouching were more resistant to light-induced fading than the albumen image itself (Stulik and Kaplan, 2013).

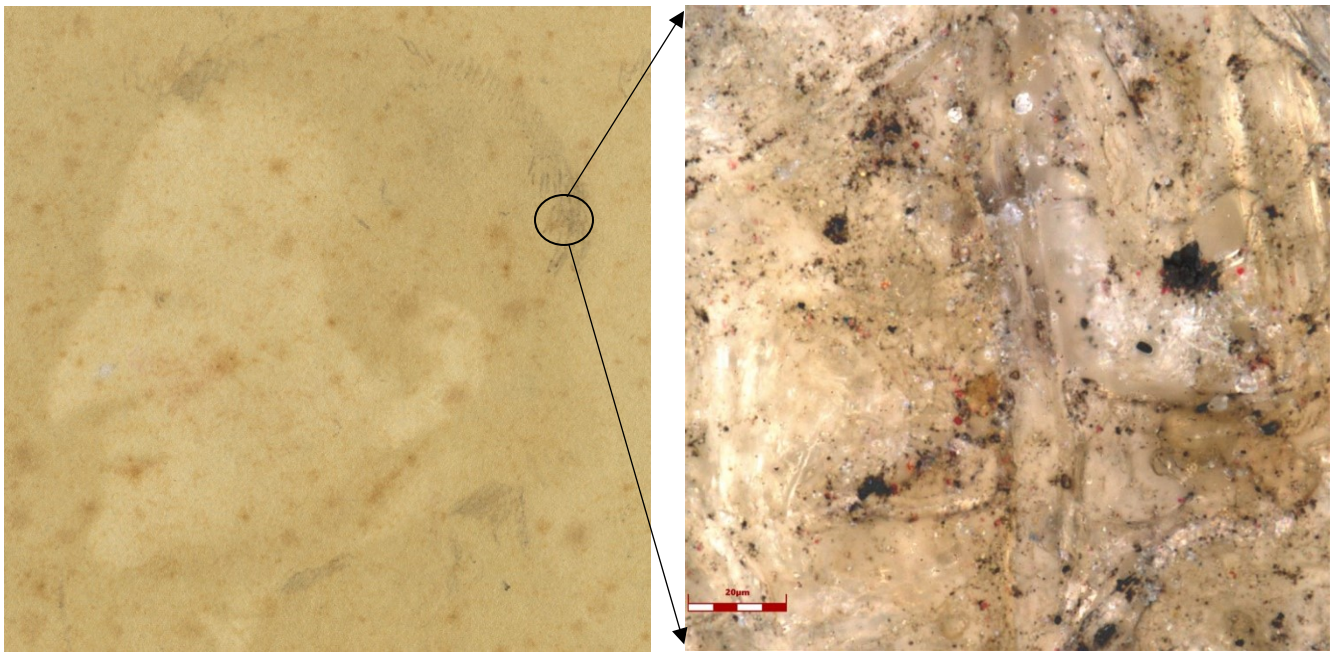

Fig. 16. Confocal microscopy: black graphite spots embedded in the glossy surface of the photographic layer. Scale bar is 20 µm.

3.1.3 Thickness Measurement

Using a confocal microscope, we were able to accurately measure the thickness of the photocard layer and the brown support. Even by examining the physical sample, it was possible to get a general idea that the brown support was probably thicker than the photocard. As mentioned earlier in Chapter One, photographs made using the albumen printing process were often mounted on a thicker support because the photographic paper was very thin and had a tendency to curl inward. A similar tendency to curl can also be observed in gelatin prints**,** which may indicate the presence of a varnish or coating on the surface of the photograph (Stulik and Kaplan 2013).

In the Figure 17, not only can the glossy surface of the photocard and the uneven distribution of the binder be observed, but the greater thickness of the brown support layer compared with the photocard layer is also clearly visible. Using a confocal microscope, the thickness of each layer was measured at three different points. The thickness of the brown support layer at the three points was 130.77, 126.16, and 129.20 μm, respectively, while the thickness of the photocard layer was 72.29, 79.11, and 77.83 μm, respectively. The resulting average thickness was approximately 128 μm for the brown support layer and 76 μm for the photocard layer. Due to the heterogeneous texture of the paper in both layers, as well as the uneven distribution of the binder in the photocard layer, the thickness measurements varied from one point to another. Therefore, the average thickness was calculated from the three measurements for each layer.

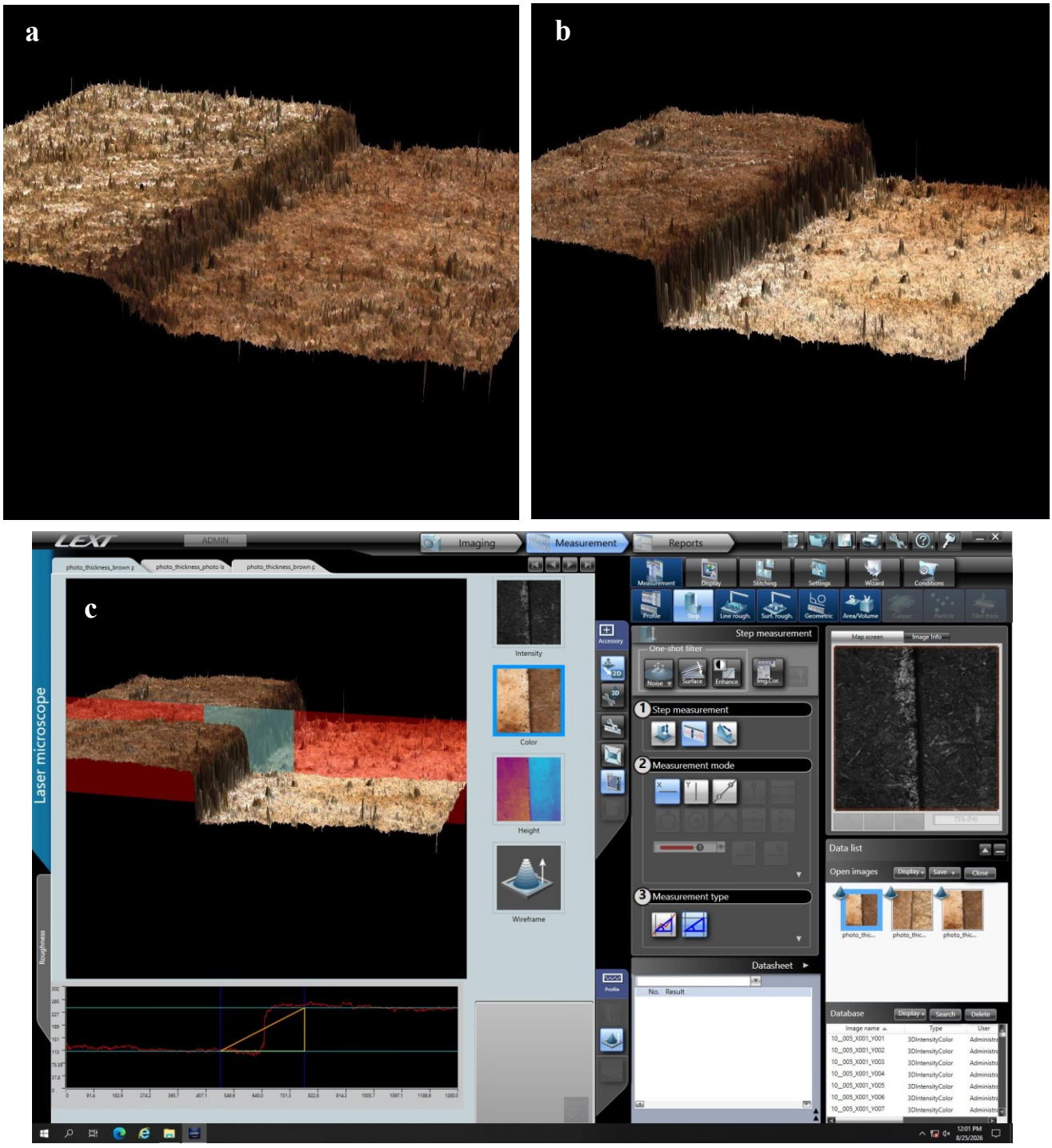

Fig. 17**.** Confocal microscopy images showing: **(a)** the glossy surface of the photocard layer in contrast to the matte surface of the brown support, together with the uneven distribution of the binder; **(b)** the thickness of the brown support layer in relation to the underlying white support; **(c)** measurement of the thickness of the photographic layers using confocal microscopy and Lext software.

3.2 ATR- FTIR

Infrared spectroscopy has been widely applied in historical photography conservation to examine chemical structures. To differentiate the binder and related organic functional groups in the photographe ATR-FTIR method was used. The main limitations of ATR-FTIR are the small area of the photograph that can be examined and the pressure required to make proper contact with the crystal, which may scratch or damage the photograph's surface (Oravec 2019). In addition, the size of the photograph prevented us from positioning certain areas, such as the subject's face and hair, under the crystal. Therefore, the analysis was limited to the edges of the photographic card and brown support.

Fig. 18. Nine points chosen on the photo sample for the ATR-FTIR measurements. Black point from photo card. Red points over browm support and blue points on white support. Points with foxing alteration are marked.

As shown in Figure 18, nine points were selected for ATR-FTIR analysis. The circled areas show the approximate locations of the selected points, while the actual areas analyzed were much smaller. The three black points correspond to the photographic card, the three red points to the brown support, and the three blue points to the white support. For both the brown and white supports, two of six selected points were located in the fixing areas. We aimed to select all three points on the photographic card from areas without foxing marks.

"**Photo Card**"

Figure 19 displays the ATR-FTIR spectra of three black points on the photo card. These bands exist at almost the same locations in all three spectra, making them extremely similar. O-H stretching vibrations from cellulose, N-H stretching vibrations from proteinaceous material, or a combination of both is responsible for a strong, broad absorption band at about 3271 cm^{-1}. A similar condition is seen for the band at about 2898 cm^{-1}, which may include contributions from both cellulose and proteinaceous material and can be attributed to C–H stretching vibrations. According to reference, proteins are characterized by the presence of a strong carbonyl (C=O) streching band referred to Amide I and an additional bending band referred to Amide II which is a combination of C-N and N-H vibrations near 1650 and 1550 cm^{-1} respectively (Derrick et al. 1999). As shown in the spectrum, the two distinct bands at 1640 and 1539 cm^{-1}, assigned to Amide I and Amide II, respectively, indicate the presence of proteinaceous material in the photograph. These two spectral

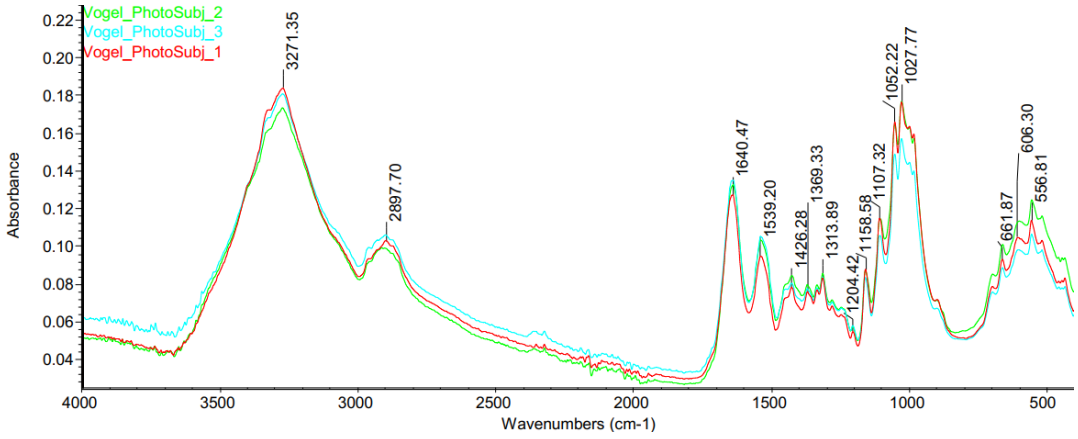

Fig. 19. ATR-FTIR spectrum of the photographic layer. It shows clearly the significant amount of the amide components in the photographic layer

peaks are typical for a number of different proteins including albumen, gelatin, casein, etc (Stulik and Kaplan 2013). One of the main challenges in this analysis was determining whether the binder used in the photograph was gelatin or albumen. To differentiate between these two proteins a detailed observation of specteral region between 1470 and 1250 cm^{-1} is needed .

According to earlier research on albumen and gelatin photographic prints, the albumen image displays two C-H bending bands of comparable intensity at roughly 1448 (Amide III) and 1385 cm^{-1}, while the gelatin image displays three C-H bands at roughly 1442 (Amide III), 1401, and 1329 cm^{-1}, which, together with the Amide I and Amide II bands occur in a stair-step pattern (Derrick 1999). The first two bands in the gelatin spectrum have different intensities. The band at 1442 cm^{-1} is generally more intense than the band at 1401 cm^{-1} (Fig. 20) (Stulik and Kaplan, 2013). However, a closer look at the ATR-FTIR spectra of the photocard in Figure 21 shows that most of the bands previously reported for gelatin and albumen in the 1470–1250 cm^{-1} region are not observed in the sample. In addition, the overall pattern of bands between this region corresponds more closely to that of cellulose. Comparison with the reference ATR-FTIR spectrum of cellulose obtained from both IRUG database (Fig. 22 and 23) and previous studies (Fig. 24) show a close match in this region, supporting the assignment of these bands mainly to cellulose.

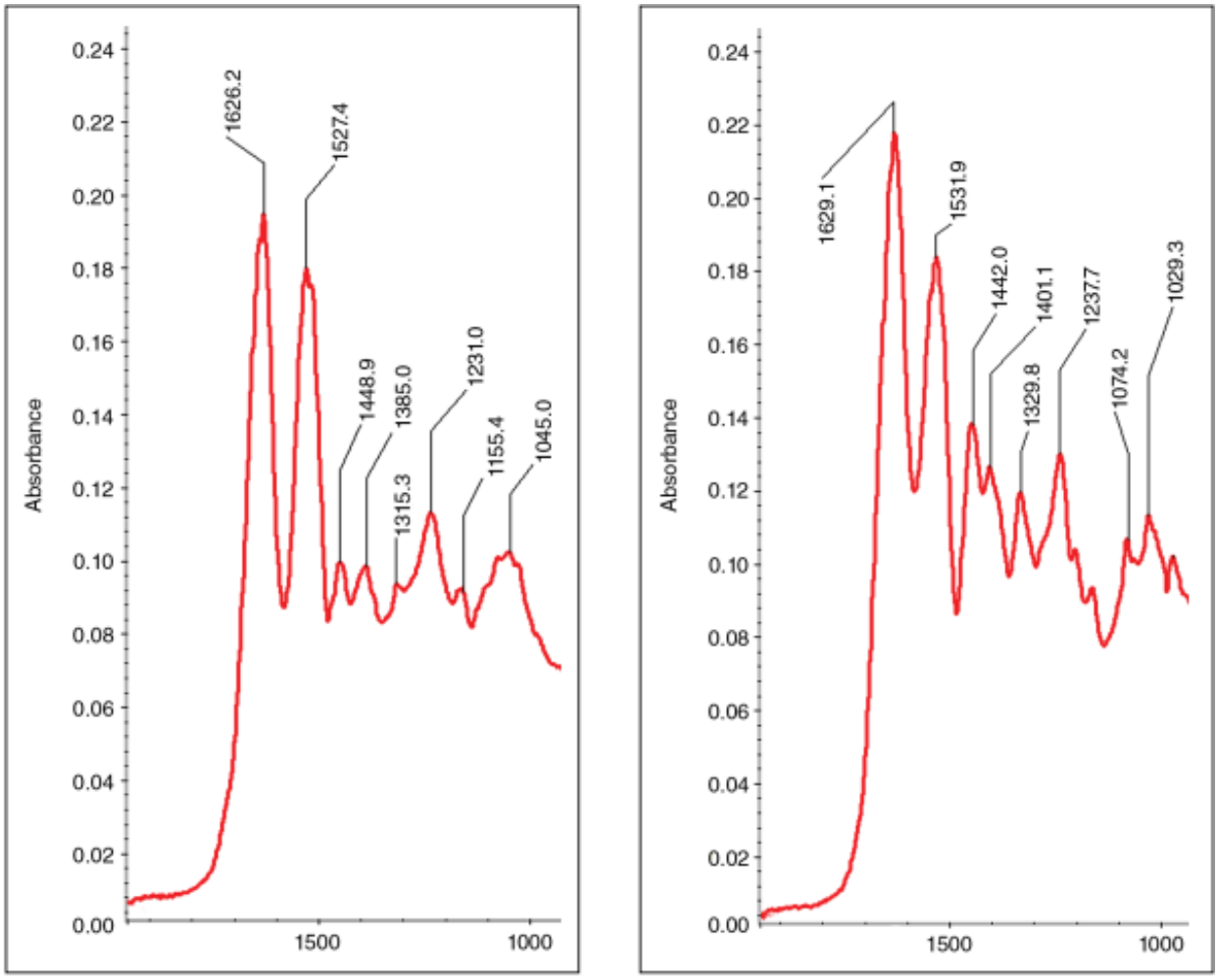

Fig. 20. Detail of the 1470 to 1250 cm^{-1} spectral region of (a) albumin, (b) gelatin (from Stulik and Kaplan 2013)

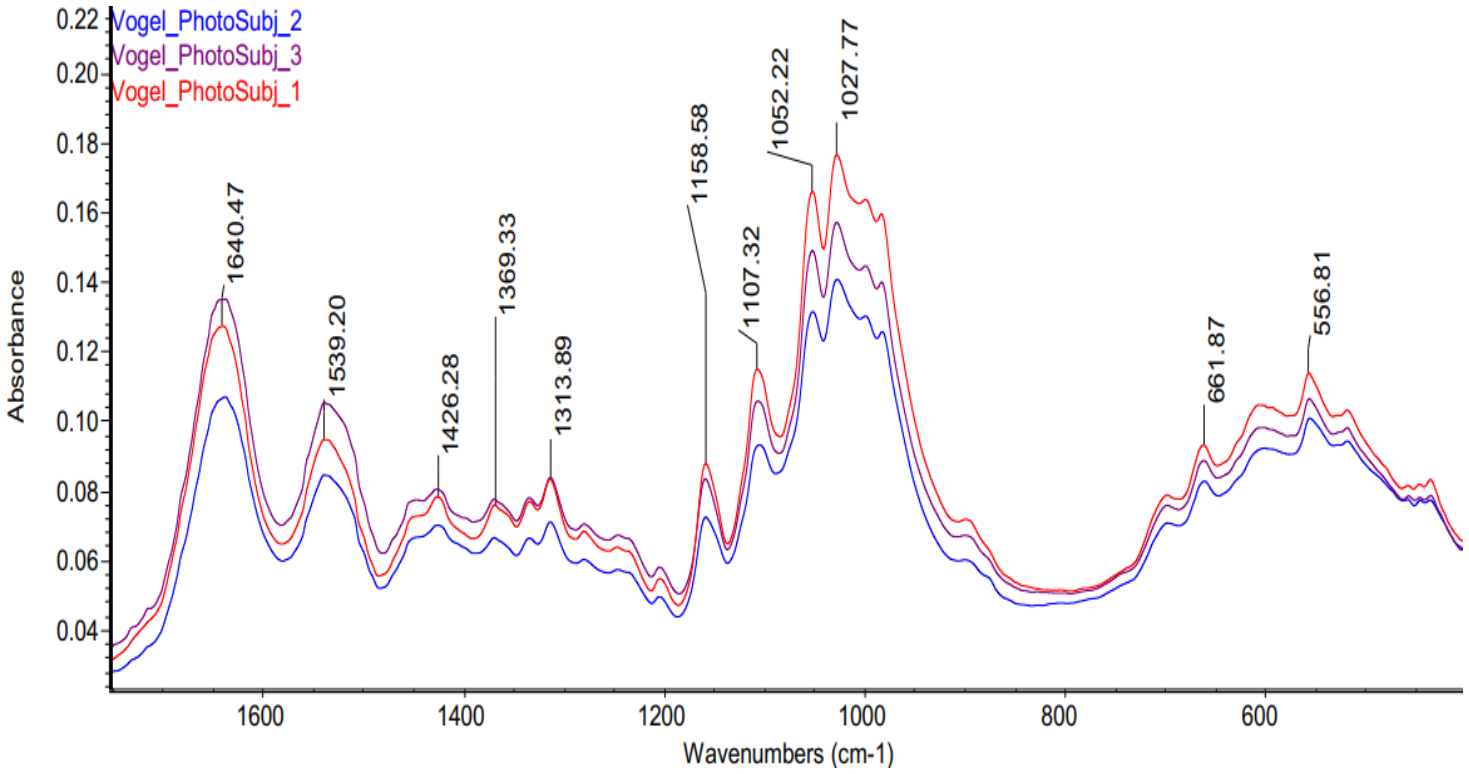

Fig. 21. ATR-FTIR spectrum of 1700 – 500 cm^{-1} region in the photographic layer shows clearly the Amide I, Amide II, and peaks related to cellulose.

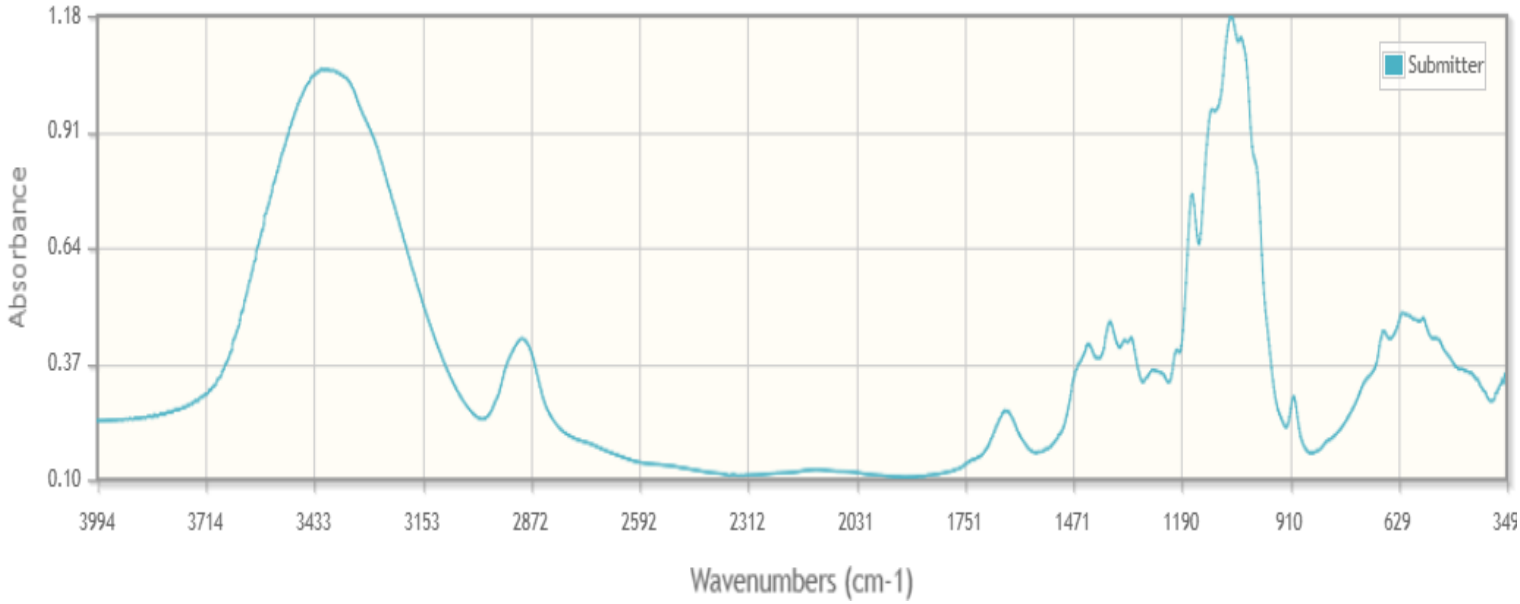

Fig. 22. FTIR spectrum of cellulose (IRUG Database 2000).

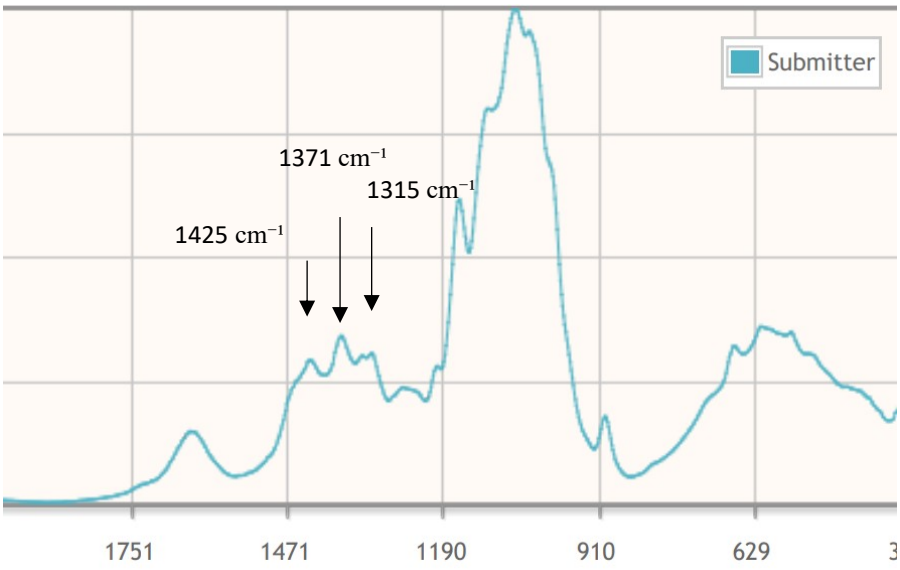

Fig. 23. ATR-FTIR spectrum of 1700 – 600 cm^{-1} region of cellulose (IRUG Database 2000).

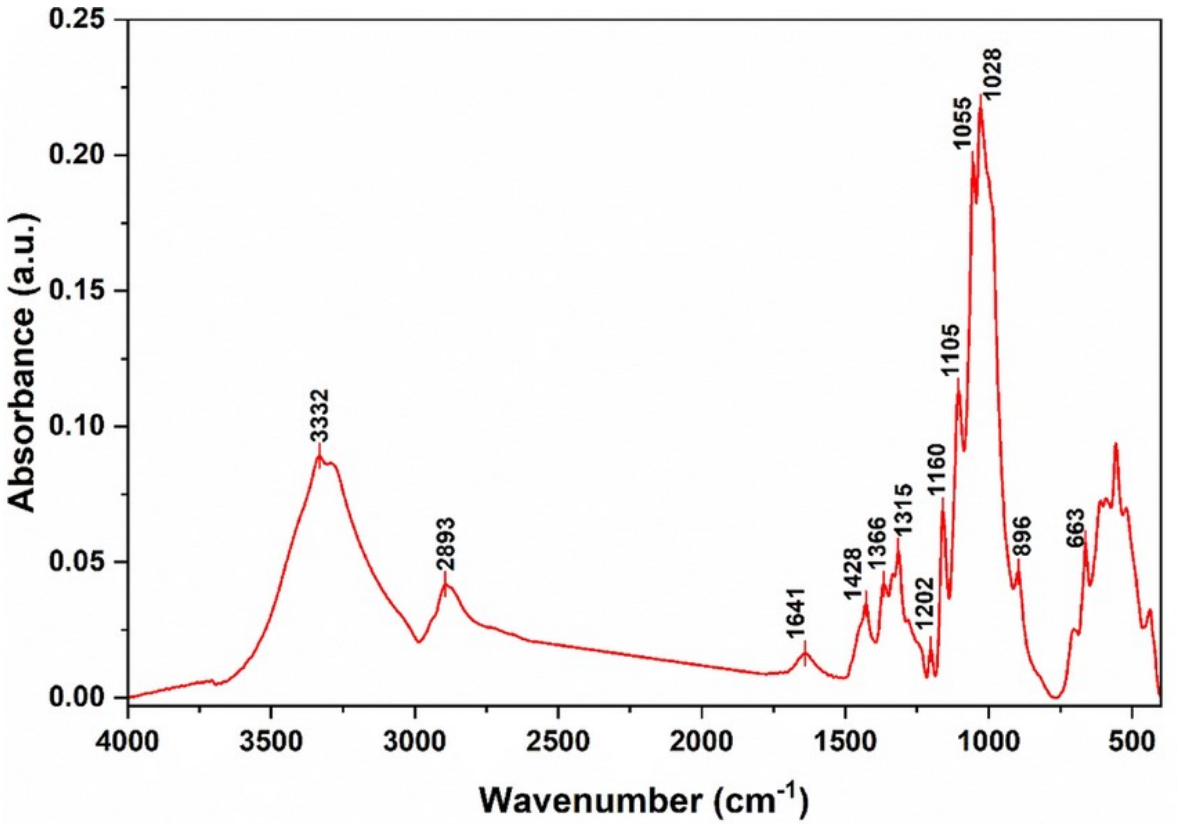

Fig. 24. ATR-FTIR spectrum of cellulose (from Refaat et al. 2023)

Moreover, the cellulose paper support can usually be seen in the spectrum as a group of C-O bending bands between about 1250 and 850 cm^{-1}. The relative thickness of the protein layer can be estimated by comparing the intensity of the Amide I band around 1630 cm^{-1} with the cellulose signal near 1020 cm^{-1}; as the protein binder becomes thicker, the cellulose signal becomes weaker (Stulik and Kaplan 2013). In the photo card layer, the main cellulose bands between 1250 and 850 cm^{-1} are quite strong and the protein-related bands in the 1470–1250 cm^{-1} region are not clearly distinguishable. Instead, the bands observed in this region are more consistent with cellulose. This suggests that the photograph probably does not contain a high concentration of protein-based binder (Stulik and Kaplan 2013).

"**Brown support**"

As mentioned earlier, albumen photographs were usually made on very thin paper and therefore tended to curl easily. To prevent this, they needed a support and often mounted on a thicker one like brown layer in investigated photo with thickness around two times more than photo card layer. As we expected this underlying brown support did not show any strong, clear signs of proteinaceous material (Fig. 25) as same as photo card layer.

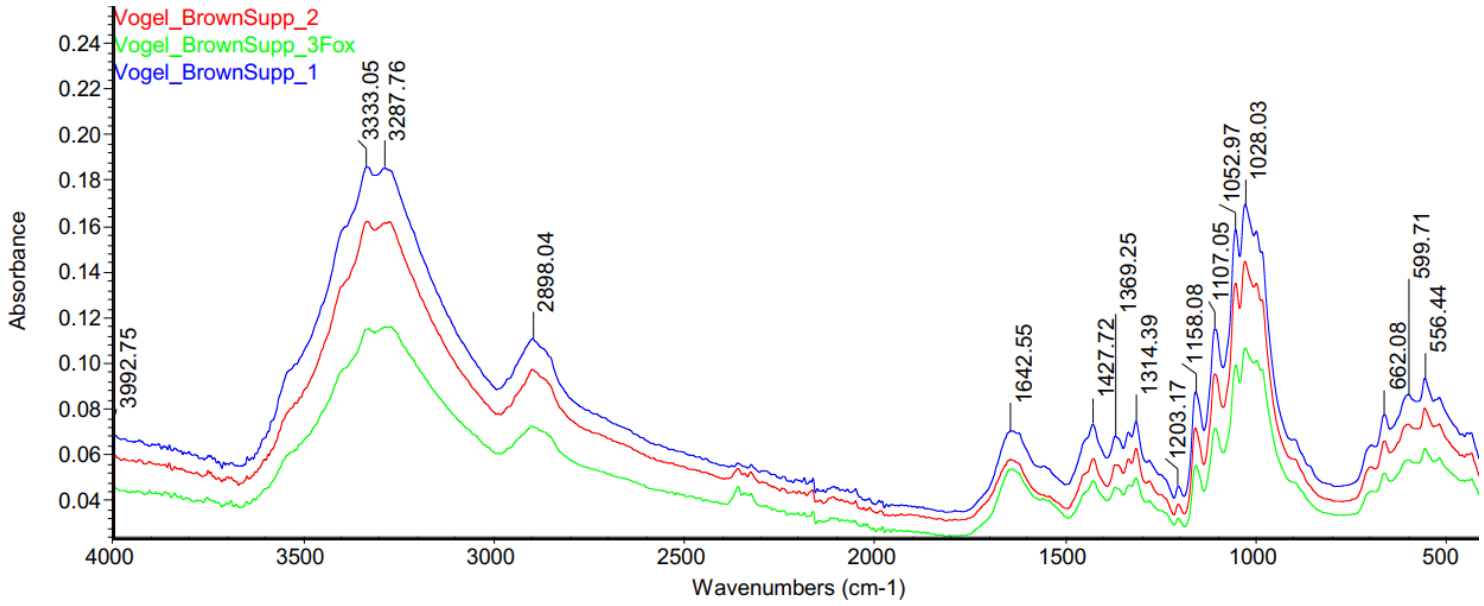

Fig. 25. ATR-FTIR spectrum of the brown support layer from 2 non-foxing and one foxing point. The peaks corresponding to cellulose are clearly dominant.

The three spectra obtained from the brown support also show a similar spectral pattern. However, the spectrum collected from the foxed area has a lower overall intensity, which may be due to weaker contact between the sample surface and the ATR crystal. As mentioned in the discussion of the photocard, the strong, broad band between 3600 and 3000 cm^{-1} is attributed to O–H stretching vibrations of cellulose. However, in the spectra obtained from all three points, several weak shoulders can also be observed on the high-wavenumber side of this broad band may be related to overlapping O–H contributions associated with different hydrogen-bonding environments (Paladini et al. 2020). The band at around 2898 cm^{-1} can be attributed to C–H stretching vibrations of cellulose.

All three spectra obtained from the brown layer show a band at around 1640 cm^{-1} with a weak intensity. Two possible interpretations can be considered for this band. If the very weak shoulder on its right side is disregarded, the band at around 1640 cm^{-1} can be attributed to absorbed water in cellulose, which is commonly observed in the region of 1635–1650 cm^{-1} (Garside and Wyeth, 2003; Derrick et al.,1999). On the other hand, if this weak shoulder is taken into account, the band at around 1640 cm^{-1} and the shoulder can be considered as Amide I and Amide II, respectively, which may be related to gelatin sizing used in papermaking (Wagner et al. 2019)

As shown in Figure 26 and 27, ATR-FTIR spectra were collected from all three layers of the photograph. Signals in the 1650–1500 cm^{-1} region can be observed in the spectra, although their intensities vary between the layers. In the brown support, a very weak shoulder appears at around 1570 cm^{-1} on the lower-wavenumber side of the 1642 cm^{-1} band, whereas this shoulder is difficult to distinguish in the white support. For all three points measured on the brown layer (red points), the band at around 1642 cm^{-1} has a weak intensity. In comparison, the same band is twice more pronounced at all three points measured on the photographic layer (black points), while its Amide II band has a lower intensity. The greater intensity of these two signals, attributed to Amide I and Amide II in the photographic layer, suggests a higher amount of proteinaceous material at the photo surface than in the brown support (Wagner et al. 2019).

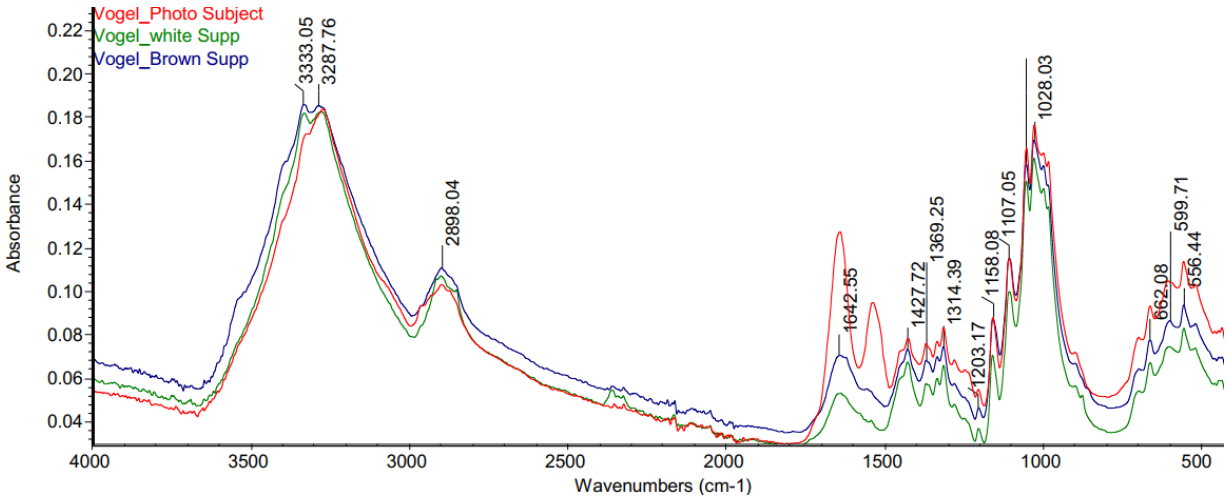

Fig. 26. ATR-FTIR spectrum of the three layers of photo shows Amide I and II in photo card layer compared to two other layers.

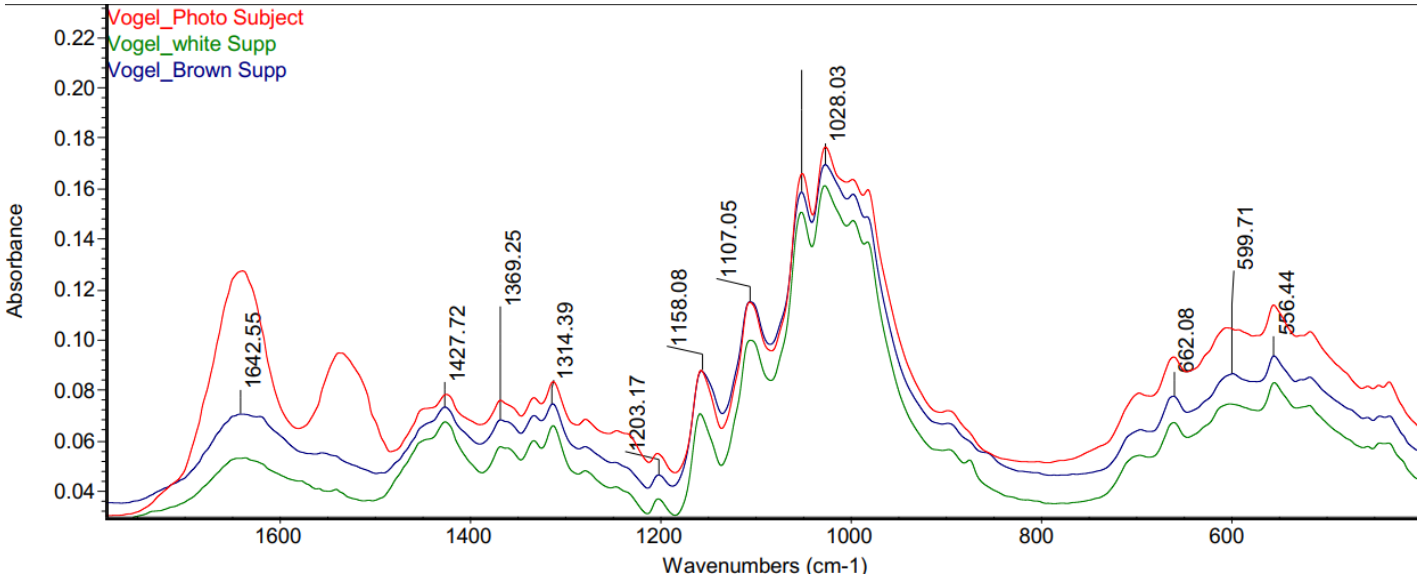

Fig. 27. Expansion of the ATR-FTIR spectrum of the three layers of photograph in the 1700- 500 cm^{-1} region.

"White Support Layer"

Comparison of the ATR-FTIR spectra obtained from the three points on the white support shows a close agreement between all three spectra, including the two non-foxed areas and the foxed area (Fig. 28). A comparison of the ATR-FTIR spectra of the white and brown supports (Fig. 27) showed that the main difference is the absence of a clearly distinguishable signal around 1570 cm^{-1} on the lower-wavenumber side of the band at approximately 1637 cm^{-1} in the white support. As discussed above, the feature near 1640 cm^{-1} may arise from water absorbed by the cellulose, which typically gives an absorption in the 1635–1650 cm^{-1} region. Moreover, the spectra obtained from all three points of this layer also show a close match with the reference ATR-FTIR spectrum of cellulose in Figure 24.

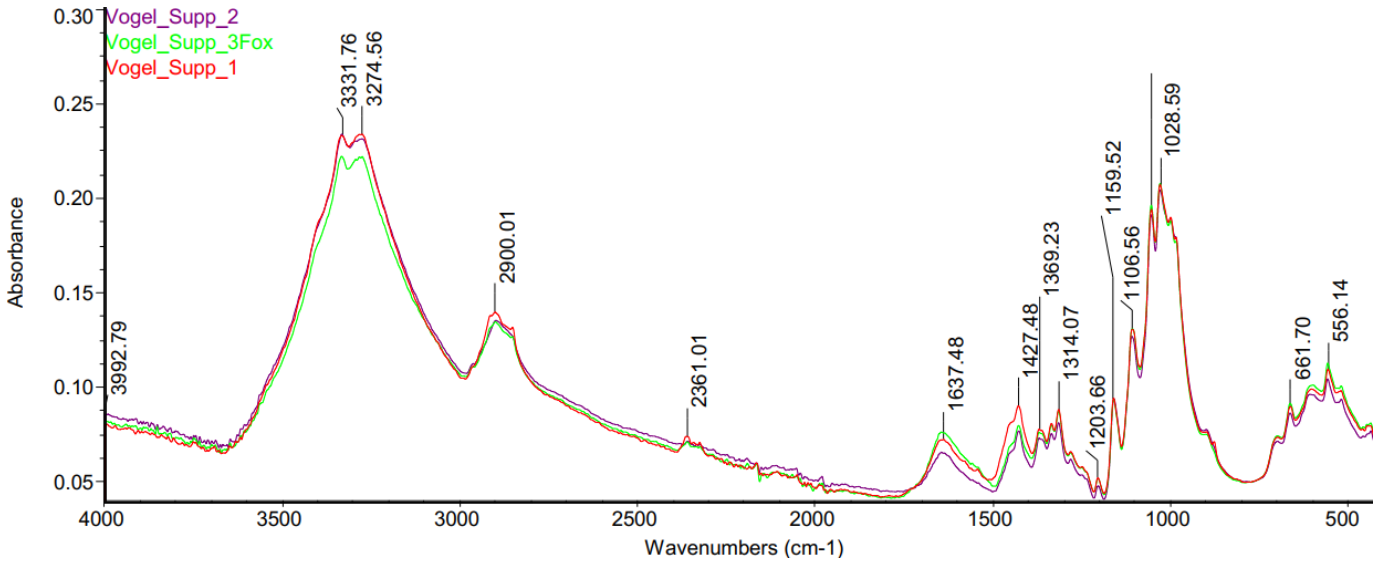

Fig. 28. ATR-FTIR spectrum of the white support layer from three measured points; one foxing and two non-foxing area

3.2.1 Micro-FTIR

Following the ATR-FTIR analysis, micro-FTIR was used to take a closer look at other points of the photo. The micro-FTIR spectra were then compared with the ATR-FTIR results to see whether the same main bands could be observed and to examine any local differences. Since the micro-FTIR measurements were carried out in external reflectance mode, some differences in band shape and relative intensity were expected. Unlike ATR-FTIR, micro-FTIR provided better flexibility in selecting the measurement areas, hence it was possible to analyse the points were closer to the photographic subject, which could not be examined by ATR-FTIR. For micro-FTIR, five points were selected overall (Fig. 29). Three black points on photocard: one selected from the retouched part over the hairs of the subject and two others in non-foxing areas. In the brown layer, two red points were chosen from non-foxing points and one extra is exacly the same foxing point from this layer investigated by ATR-FTIR.

It is important to mention that the ER-FTIR spectra were converted from reflectance to pseudo-absorbance using A=log(1/R), where R is the measured reflectance. Because ER-FTIR is affected by reflection phenomena, absorption bands may appear inverted or derivative-shaped, and artificial pseudopeaks may also occur near the edges of strong bands. As a result, the apparent band positions may differ from those observed in ATR-FTIR (Geminiani et al. 2025).

Fig. 29. The five points on photo card and brown support layer investigated by ER-FTIR

"**Photo card**"

As shown in Figure 30, the ER-FTIR spectrum of the photo card layer provides the key peaks needed to identify the proteinaceous material present in the photograph. Compared with ATR-FTIR, Amide I showed a shift of approximately 40 cm^{-1}, appearing at 1685 cm^{-1}, while Amide II shifted by about 25 cm^{-1}, appearing at 1563 cm^{-1}. These positions of the Amide I and II bands in the ER-FTIR spectra showed a marked difference from those observed in ATR-FTIR. This behavior is consistent with previous studies on egg-white binders, which have shown that reflection effects in ER-FTIR can alter the apparent positions of protein-related bands (Nodari and Riccardi 2019).

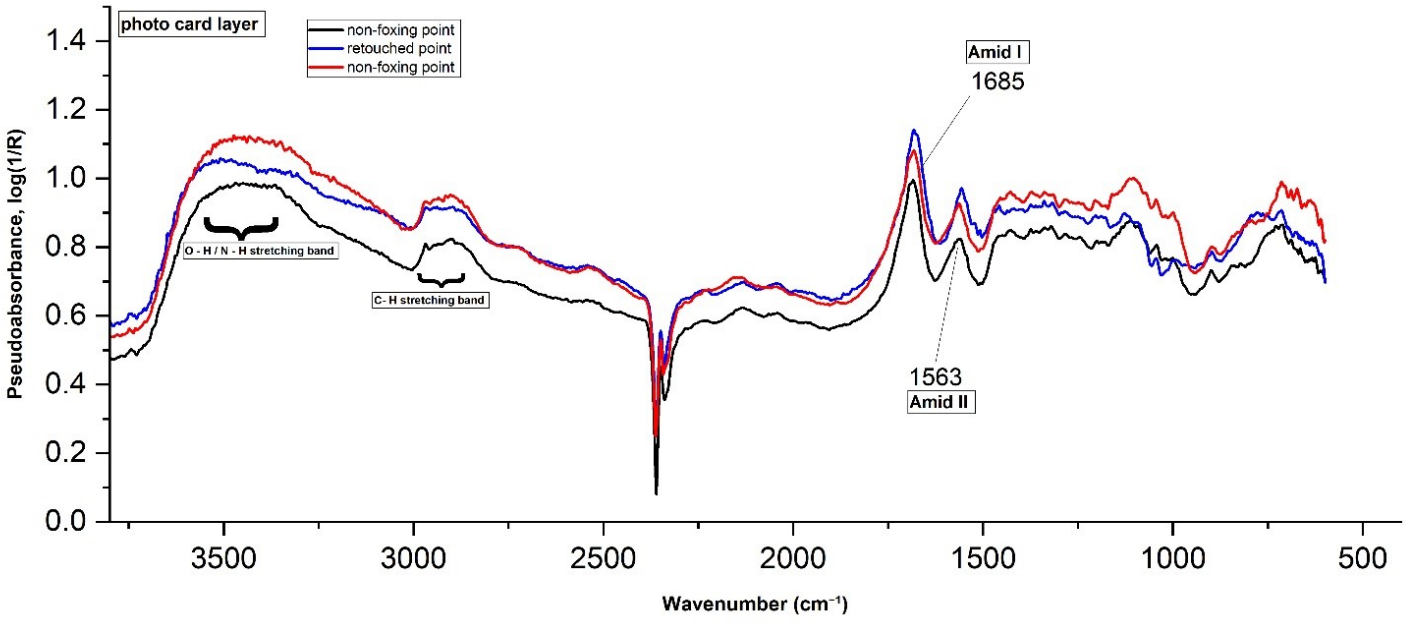

Fig. 30. ER-FTIR spectra of photo card layer from three points; one retouching(blue) and two non-foxing areas(black and red) show both Amide I and II in all three points. The region of proteinous peaks masked peaks of cellulose between 1500- 1000 cm^{-1}

One of the noticeable differences between the ER-FTIR and ATR-FTIR spectra of the photocard layer was that, in the ATR-FTIR spectrum, the C–H and CH_2 deformation bands in the 1500–1200 cm^{-1} region, as well as the main cellulose absorption region between approximately 1200 and 900 cm^{-1}, were clearly visible and readily identifiable. According to previous studies, in the albumen print, cellulose is visible in the ATR-FTIR spectrum because the albumen layer is thin. In contrast,

it is barely detected in ER-FTIR, since the response in external reflection is strongly influenced by the specular reflectivity of the different layers. As a result, the thin and glossy albumen layer can dominate the ER-FTIR spectrum and largely mask the contribution from the cellulose support and making it more difficult to identify (Walker and Berrie 2023). In the ER-FTIR spectrum, much of the cellulose signal is obscured by the Amide bands of the protein binder in the 1690–1470 cm^{-1} region. Only weak features attributable to cellulose can be seen between about 1130 and 700 cm^{-1}, but they are too faint for a confident identification (Freixas-Jambert et al. 2024). The ER-FTIR spectrum of the retouched area showed Amide I and Amide II at about the same positions as in the other two areas. In the cellulose region, as was also observed at the other two points, the bands were much less distinct, and the spectrum appeared noticeably flatter.

"**Brown support layer"**

After examining two non-fixing points on the brown support layer and comparing their ER-FTIR spectra with that of a modern paper sample, a clear similarity between the spectra was observed (Fig. 31). In contrast to the previous spectrum, all the characteristic cellulose bands in Figure 31 were clearly visible and could be identified. A broad OH stretching band is observed around 3460 cm^{-1}. The region between about 2970 and 2860 cm^{-1}, with a broad band centred near 2903 cm^{-1}, is related to the asymmetric and symmetric stretching vibrations of CH_3 and CH_2 groups. Bands at 1434, 1372, 1338, and 1323 cm^{-1} are associated with CH_2 and CH bending vibrations. The band at 1648 cm^{-1} is attributed to combined C=O and H–O–H vibrations. The region between 1180 and 1040 cm^{-1} is mainly related to C–O and C–C stretching in the cellulose chain. A small band near 1000 cm^{-1} can also be assigned to C–O stretching, while the peak around 896 cm^{-1} is associated with C–O–C deformation and is characteristic of the amorphous region of cellulose (Freixas-Jambert et al., 2024)

In the modern paper spectrum, the bands at approximately 1794 and 872 cm^{-1} were the only prominent features that were not observed in the two spectra of the brown support paper. The region between 2000 and 2300 cm^{-1}, which is generally associated with the stretching vibrations of triple bonds, such as C≡C and C≡N, can be observed in all three ER-FTIR spectra. These bands may not be observed in the ATR spectrum, as ER-FTIR and ATR do not generate spectra through the same mechanism. However, in ER-FTIR spectra, particularly for heterogeneous and layered

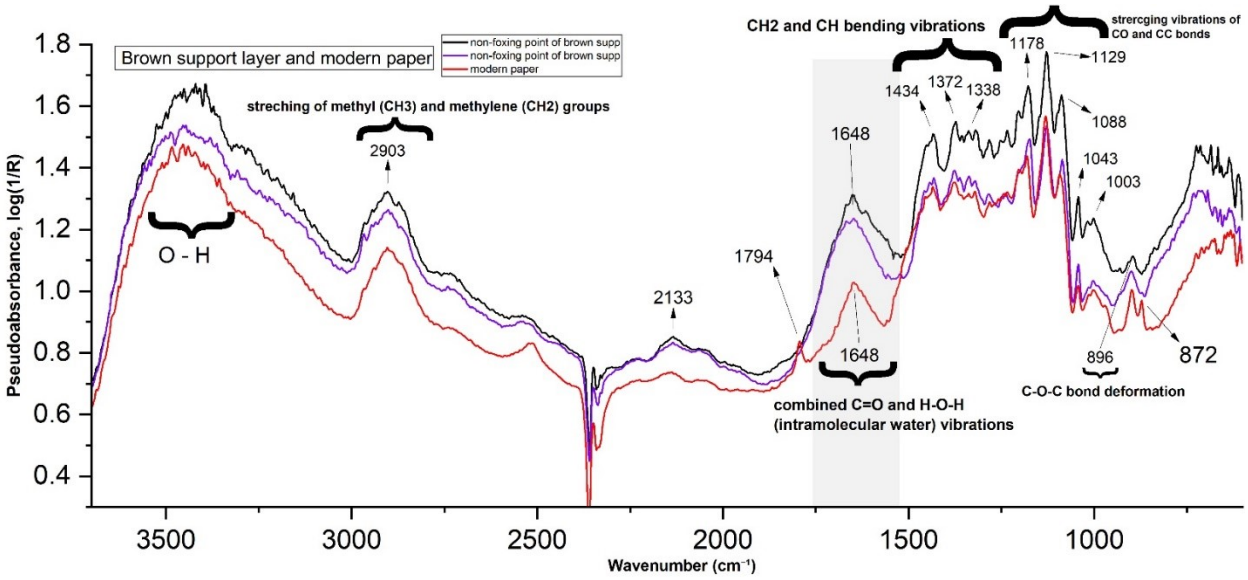

Fig.31. ER-FTIR spectrum of brown support layer from two non foxing points. Acomparison between modern paper and historical brown layer of photo presents the similarity between two papers.

materials such as paper, reflective phenomena and combination/overtone bands may also produce or enhance features in this region. Therefore, their assignment should be made with caution and considered alongside the other bands present in the spectrum.

The relatively sharp peak at 1794 cm^{-1} in modern paper may also be associated with the presence of mineral additives, such as calcium carbonate ($CaCO_3$), which has been used in papermaking to increase whiteness and reduce acidity.

The highlighted region shows the same band position at around 1648 cm^{-1} in all three spectra. The main differences are the lower intensity and sharper shape of this band in the modern paper, whereas the historical brown support shows a stronger and broader band. Thess differences may suggest the possible presence of proteinaceous sizing in the brown paper. However, the absence of a clearly identifiable Amide II band in the ER-FTIR spectrum does not allow the presence of proteinaceous sizing to be confirmed conclusively. Moreover, the detection of the Amide II band using this technique can be difficult, which may also explain its absence from the spectrum. The weaker features observed on the right-hand side of the Amide I region can therefore only be considered as supporting evidence for its possible presence.

On the other hand, comparison of the ER-FTIR and ATR-FTIR spectra collected from the same foxing point on the brown support layer gave a different , interesting result (Fig. 32).

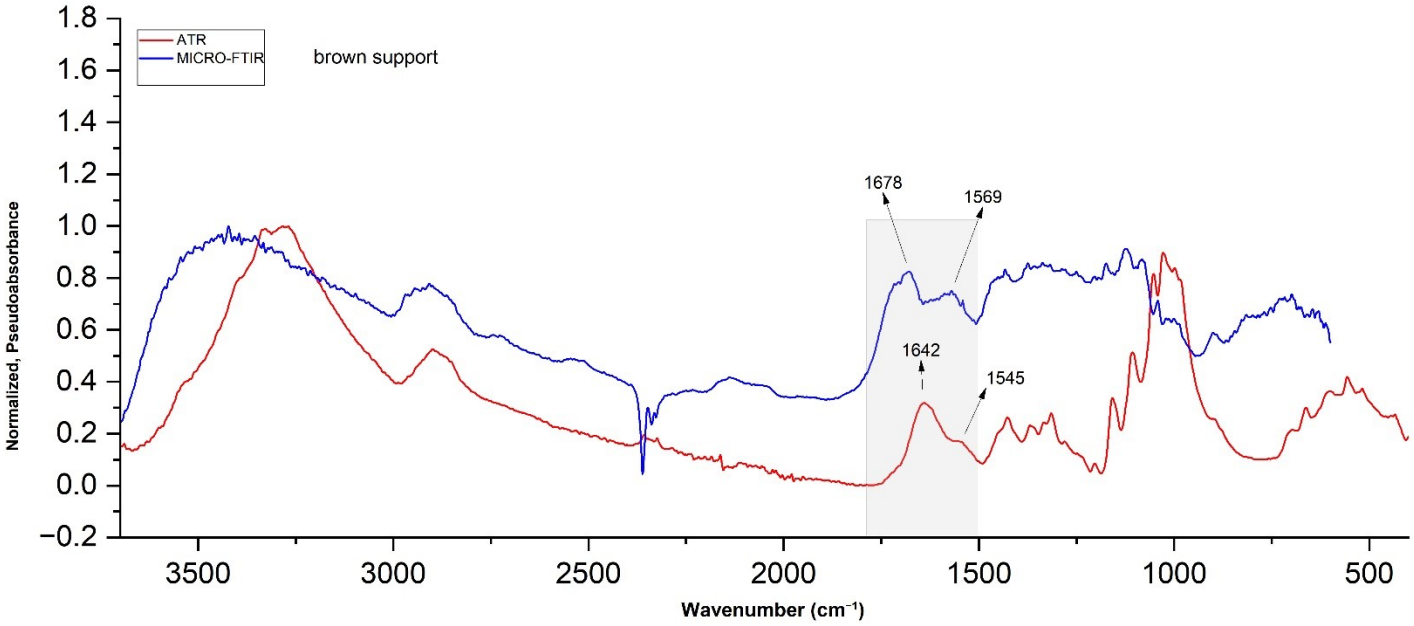

Fig. 32. Comparison between ER-FTIR and ATR-FTIR spectrums of a non-foxing point on brown support layer

As mentioned earlier, the ATR-FTIR spectrum of the foxed point on the brown support showed a band at around 1640 cm^{-1} with a shoulder near 1545 cm^{-1}. In contrast to the non-foxed areas, ER-FTIR measurements of the same point revealed two clearly resolved bands at 1678 and 1569 cm^{-1}. A review of previous studies on foxing in historical paper did not provide a clear explanation for these differences, as most investigations were based on ATR-FTIR rather than external reflection measurements. Previous ATR-FTIR studies have reported changes in the 1500–1200 cm^{-1} region at foxed areas, where fungal material may produce a broad plateau due to several overlapping bands (Zotti et al. 2011). In the present study, however, the ATR-FTIR spectrum of the foxed point showed no noticeable change in this region compared with the non-foxed point. In the corresponding ER-FTIR spectrum, on the other hand, the individual features within this region were less clearly resolved and more difficult to distinguish than those observed at the non-foxed areas. Since investigating the origin of foxing and the associated changes occurring at the paper

surface was beyond the scope of this study, these observations could be explored further in future research.

3.3 XRF

Although XRF cannot directly identify the organic compounds present on the surface of a photographic print, the data it provides can still be very useful. By comparing XRF results with published studies, researchers can identify specific marker elements that may be linked to particular photographic processes (Modica et al. 2017). For the XRF analysis, several measurement points were initially selected across the circular photocard and brown support. Each point was analyzed for 120 s using a tube voltage of 40 kV and a current of 100 µA. Because the photograph is severely faded and affected by surface degradation, the spectra collected from the white areas (Dmin) and dark areas (Dmax) regions were, in most cases, very similar and showed no clear differences even with increasing the acquisition time to 240 s and the tube voltage to 50 kV to obtain more differences. To make the experimental conditions consistent for both the photocard and the brown support, one point on the brown support (Fig 33) was selected and measured using the new conditions of 240 seconds and 50 kV. The results could then be compared with those obtained from the photocard. In addition, one point was measured on the white support on the reverse side of the photograph, allowing comparison with the measurements obtained from the other two layers.

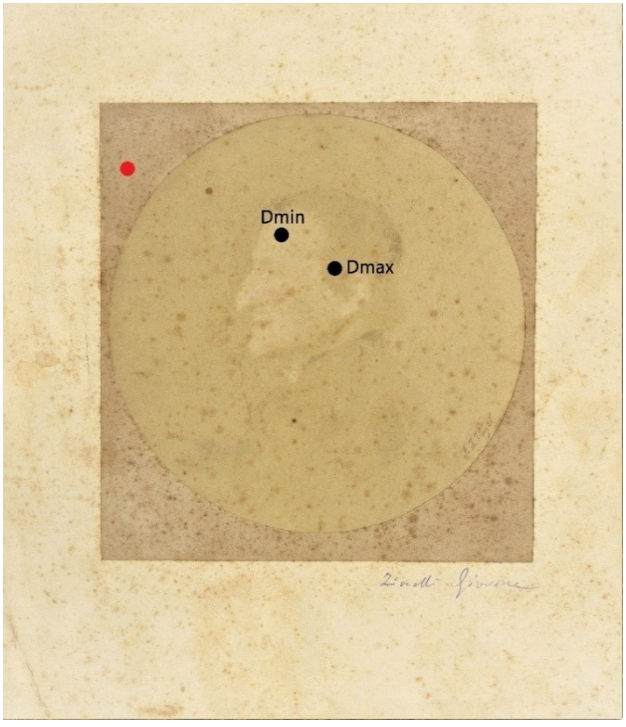

Fig. 33. Two points (black) from clear (Dmin) and dark (Dmax) areas of the of photographic layer, and one point (red) from the brown support analyzed by XRF.

“ Photo card ”

A representative spectrum for both Dmin and Dmax (black spots) obtained by the XRF analysis indicates the presence of Fe, K, Ca, S, Zn, Ni and Mn (Fig. 34). For each identified element, the background-corrected net peak area was determined from the Dmin and Dmax spectra and used as a semi-quantitative measure of the XRF signal intensity. The resulting values are presented in Table 1.

Based on previous studies of historical photographs, several elements are considered particularly important for distinguishing between albumen prints and silver gelatin prints such as Ag, Ba, Sr, S, and Au. Since silver is the imaging element used in black-and-white photographs, we expected to see a relatively strong silver peak before carrying out the analysis. However, the spectra did not provide clear evidence for the presence of silver in the sample. The silver appears in the long measurements at 22.16 KeV (Ag Kα), as a weak peak slightly above background (Fig. 35). A relatively strong peak was observed around 2.98 keV, which corresponds to the Ag Lα line. However, this line strongly overlaps with the Ar Kα line at about 2.96 keV, so the peak cannot be fully interpreted, however it is evident that the silver contribution increases in the photo layer with respect to the supporting paper (Fig. 36). The argon signal is related to measurements carried out in air. The XRF results obtained on the photo card layer reveal high counts of iron and calcium. Based on previous studies of historical photographs, high levels of elements such as Fe and Ca, together with Zn, Cu and Mn, have often been attributed to filler components in the paper support (Stulik and Kaplan 2013; Guerrero and Silva 2023). Among these elements, Fe, Ca, and Zn generally show stronger signals. Zinc, although a metal, is not considered an image-forming element or a toning agent in these photograph, but rather a component associated with the support. This is because zinc compounds were commonly used at the time to whiten paper (Guerrero and Silva 2023). In another study, the presence of Zn and Cu was considered likely to be related to impurities (Puškárová et al. 2016).

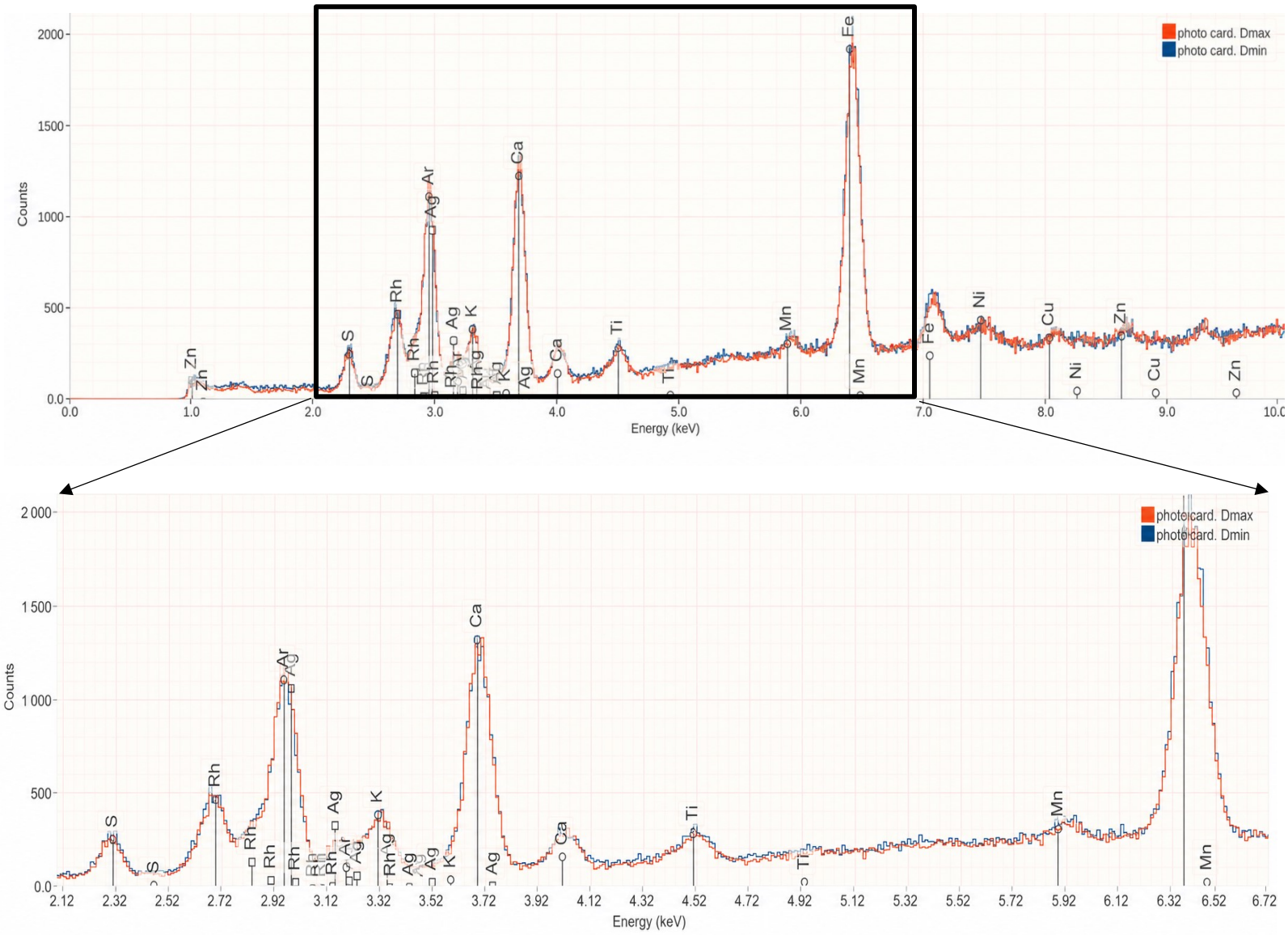

Fig. 34. pXRF spectra measured on the Dmin and Dmax of photo card layer. The major elements detected are S, K, Ca, and Fe. Most of the other elements detected at trace level are instrumental artefacts.

Table 1. Background-corrected net peak areas of selected characteristic X-ray lines in the Dmin and Dmax regions.

Element	Line examined	Energy (keV)	Dmin peak net area (counts)	Dmax peak net area (counts)	Note
Ag	Kα	22.16	Ag Kα barely above background	Ag Kα barely above background	Very weak
Ag	Lα	2.98	7348 ± 113 (Ag Lα / Ar Kα combined signal)	7876 ± 127 (Ag Lα / Ar Kα combined signal)	Strong overlap with Ar Kα
K	Kα	3.31	1738 ± 75	1575 ± 73	Detected
Fe	Kα	6.40	22211 ± 193	20938 ± 188	Strong peak
Ca	Kα	3.69	11910 ± 127	12016 ± 137	Strong peak
S	Kα	2.31	1797 ± 58	1670 ± 53	Clear peak
Ti	Kα	4.51	1715 ± 78	1704 ± 73	Possible overlap with Ba Lα
Mn	Kα	5.90	1020 ± 115	1173 ± 103	Detected; Kβ affected by Fe
Ni	Kα	7.48	797 ± 107	759 ± 103	Detected
Zn	Kα	8.64	936 ± 92	1004 ± 95	Weak to moderate
Sr	Kα	14.16	n.d.	n.d.	No clear peak
Au	Lα	9.71	n.d.	n.d.	No clear peak
Ar	Kα	2.96	–	–	Air-related signal; overlaps with Ag Lα
Rh	Lα	2.69	–	–	Signal from Rh X-ray tube
Cu	Kα	8.03	723 ± 111	788 ± 105	Weak to moderate

Note. Dmin and Dmax values were obtained from the Peak−Bkgd output using the "Integrate peak (background corrected)" function in DTSA-II. For overlapping peaks, the net area was not assigned to a single element. n.d. = not detected.

Most Gelatin silver photographs show a baryta layer, identified by the presence of barium and strontium in the XRF spectra (Stulik and Kaplan 2013). The baryta layer was commonly used to improve the appearance of the print and strengthen the paper support (Poggialini et al. 2025). The baryta layer in gelatin photographs is mainly made of barium sulfate ($BaSO_4$), with smaller amounts of strontium sulfate ($SrSO_4$) and titanium dioxide (TiO_2) (Lin Liu et al. 2024). However, no distinct Ba peak was observed. It should be mentioned, however, that the Ti Kα line at about 4.51 keV lies very close to the Ba Lα line at about 4.47 keV, so the two signals may overlap. If a Baryta layer were present, the Ba peak would be expected to be stronger and would likely be accompanied by other elements such as strontium which is absent in this layer. The presence of barium in this case may be related to $BaSO_4$ as a filler in paper and could also serve as a component or whitening agent in the paper substrate (Guerrero and Silva 2023). Another important element is sulfur, which can be found both in the baryta layer ($BaSO_4$) of gelatin prints and in albumen prints. Sulfur (S), which was detected in both Dmin and D max, may have several possible sources, including silver sulfuration, sulfur-containing amino acids in albumen, and compounds present in the primary or secondary supports (Guerrero and Silva 2023).

Gold toning was commonly used as the main toning method for albumen prints (Lin Liu et al. 2024) but the result of XRF analysis proves no trace of Au in the photo sample.

"**Brown support layer**"

In the second comparison, a point was selected on the brown support and, as mentioned earlier, it was analyzed under the same conditions as the Dmin and Dmax points on the photographic layer. As shown in Figure 35, several elements show clear differences between the brown support and the photographic layer. In particular, both the Fe Kα and Fe Kβ peaks are stronger in the brown support than in the photographic layer. This suggests a higher amount of iron in the brown support, and iron-containing compounds may also have contributed to its brown color. Another element that shows a clearly lower intensity in the brown support than in the photographic layer is sulfur. As discussed in the previous section, the higher sulfur signal in the photographic layer may be related to the presence of albumen, since egg-white proteins contain sulfur-bearing amino acids. However, sulfur alone cannot be considered a definitive indicator of an albumen print. As

mentioned in the previous section, no strong, clear Au Lα peak at 9.71 keV was observed in the Dmin and Dmax areas of the photographic layer.

The only element present in the photo layer which is not present in the supporting brown paper is silver.

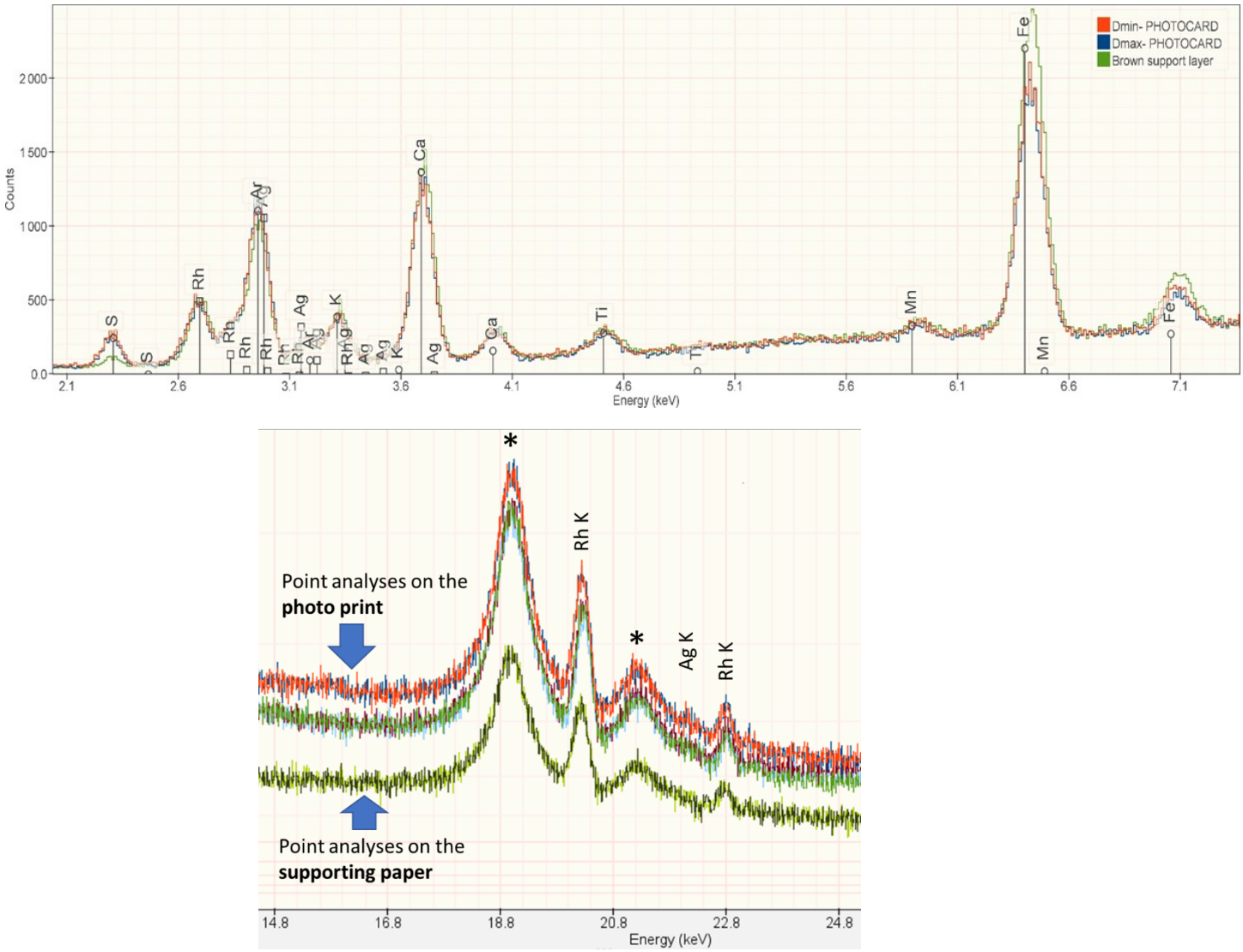

Fig. 35. Comparison between portable XRF spectrum of photocard layer and brown support shows the main different intensity in S and Fe. The Ag Kα peak is slightly visible above background only in the photo layer.

Figure 36 shows the XRF spectra obtained from one point on the photocard, one point on the brown support, and one point on the back of white support. All three points were measured under exactly the same experimental conditions. The main differences among these three layers are observed in the relative intensities of sulfur, potassium, calcium, iron, and silver.

The intensity of the sulfur peak (S Kα) at around 2.31 keV is clearly higher in the photocard layer than in the other two layers, while no noticeable difference is observed between the white and brown supports. Although the potassium peak is slightly stronger in the photocard than in the brown support, the overall intensities of both potassium and calcium are clearly higher in the photocard and brown support than in the white support.

A similar trend is observed for iron. The Fe peak intensity decreases in the order of brown support, photocard, and white support, with the difference between the brown and white supports being particularly clear in the spectrum.

Finally, the photocard layer also shows a stronger silver signal than the two support layers. Although the Ag Lα peak at around 2.98 keV overlaps with the Ar Kα peak, the Ag L-line region is still more intense in the photocard layer. In contrast, no distinct Ag Kα peak at around 22.16 keV can be identified in either the brown or white support, even at higher magnification. Under the same measurement conditions, however, a very weak signal is visible at this energy in the photocard layer

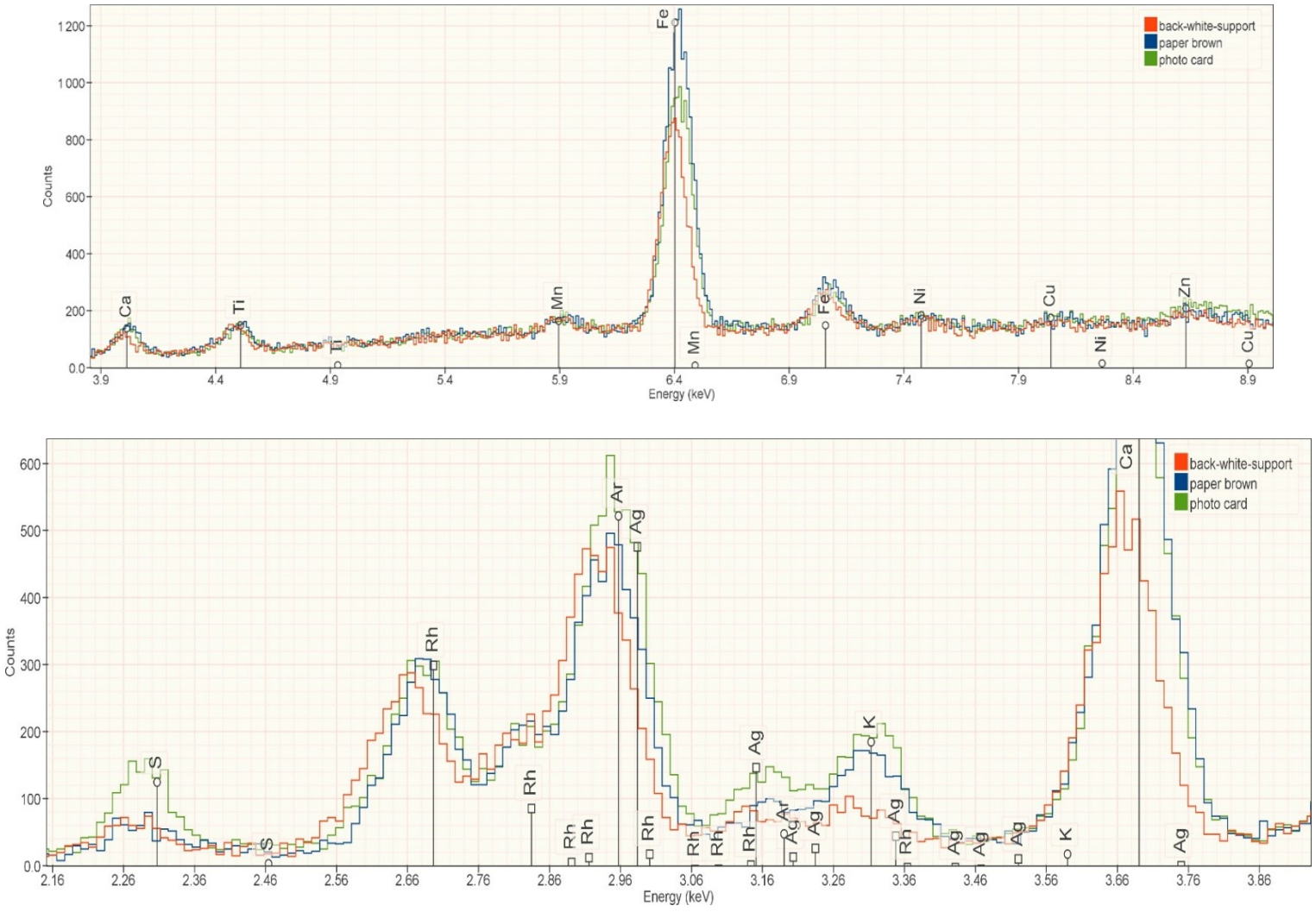

Fig. 36. The XRF spectra collected from the three layers of the photograph revealed variations in the signal intensities of elements such as S, Fe, Ca, and K**.**

4 Discussion and Conclusions

4.1 Discussion

The object examined in this study is a historical portrait photograph produced between 1850 and 1855 by the German photographer and lithographer Friedrich Carl Vogel. The portrait depicts the Venetian bishop Mons. Zanelli. The object is composed of three main layers. The first is a circular photographic layer, on which the portrait itself is printed and which is referred to here as the photocard. This circular layer is mounted onto a square brown support, and the two are in turn attached to a rectangular white support.

A first visual examination of the object reveals extensive fading of the photographic image. Many facial details, including the lips, eyes, eyebrows, and neck, are difficult to distinguish and in some areas are almost completely lost. Numerous foxing spots of different sizes and shapes are also visible across all three layers of the object. Noticeable color changes can also be observed. The originally white support has shifted toward a creamy, yellowish tone, while the circular photocard shows widespread yellowing across its surface. Taken together, these changes—including image fading, foxing, and yellowing—indicate significant alteration of the materials over time and an overall poor state of preservation.

Around the time the photograph was produced, between approximately 1850 and 1855, two photographic processes—salt printing and albumen printing—were being used and further developed by photographers and researchers in different countries. To help distinguish between these two techniques, the sample was first examined using optical microscopy and confocal microscopy, and images were recorded from different areas of the object at several magnifications. Salt prints usually have a matte appearance, with the image seeming to sink into the paper fibers rather than sitting as a glossy layer on the surface (Stulik and Kaplan 2013). For the photograph examined in this study, the circular area of the photocard has a glossy surface. This gloss is visible under normal lighting, and the microscopic images also confirmed it compared to the other two layers. In microscopic images with a 20 µm scale bar, observations from different areas of the photocard showed that the paper fibers appear to be embedded in a glossy material. This material is most likely a protein-based binder, possibly egg white (albumen) or gelatin.

In addition, microscopic examination revealed pools of binder distributed unevenly across different areas of the photocard. Tiny bubbles and small holes were visible within some of these pools, and their color also varied, appearing light brown in some areas and darker in others. Previous studies have associated these microscopic features with the presence of an albumen binder (Wagner et al 2019).

On the other hand, no network of cracks was observed on the surface of the photocard, although this is considered one of the characteristic features of albumen prints. This raised the possibility that the concentration of the protein-based binder, such as albumen, may not have been particularly high. Moreover, the image layer is neither clearly separated from the paper fibers nor deeply penetrated into them which is the characteristic of salt prints (Hill 2018). Nevertheless, albumen prints from this period did not always have a highly glossy surface or a thick, cracked, and yellowed binder layer. These features are more commonly associated with later commercially produced albumen papers. In those later examples, the image-bearing binder layer is usually more clearly visible above and distinct from the paper fibers (Wagner at al. 2019).

ATR-FTIR is widely used in the study and conservation of historical photographs because it provides a fast and reliable way to examine photographic binders. However, distinguishing gelatin from egg albumen can be difficult, as both are protein-based materials and show very similar FTIR spectra (Oravec et al. 2019). As expected, the results clearly showed the two main protein-related bands, Amide I and Amide II. However, Amide III and the series of bands in the 1500–1300 cm^{-1} region, which can be characteristic of albumen and differ from those observed in gelatin, were not detected. This can be expected when the binder concentration is low (Stulik and Kaplan 2013). The ATR-FTIR spectrum of the photocard layer instead showed strong and clearly defined cellulose bands, particularly in the 1200–900 cm^{-1} region, while the protein-related Amide I and Amide II bands were weaker.

In albumen prints, the relative intensity of the protein and cellulose bands can provide information about the thickness of the albumen layer. A thicker albumen coating tends to reduce the cellulose signal from the paper support, making the Amide I peak more prominent, as seen in albumen-rich or double-coated Albumen prints. In contrast, when the albumen layer is thin, the ATR-FTIR beam can interact more strongly with the paper underneath, resulting in more pronounced cellulose bands. Therefore, the strong cellulose signal observed in the photocard spectrum may be consistent

with the presence of a thin protein binder layer. Previous studies on albumen prints have reported a relationship between the intensity of the Amide I peak and the characteristic cellulose peak at around 1100 cm^{-1}. In prints dating from before about 1870, when highly concentrated albumen coatings were generally not used, the intensity of the Amide I peak was often very close to, or similar to, that of the cellulose peak around 1100 cm^{-1}. After 1870, as the amount or thickness of the albumen layer increased, the Amide I peak became noticeably stronger and, in some cases, exceeded the cellulose peak. The earlier technique, which became common in the early 1850s, is generally referred to as albumenized print (Stulik and Kaplan 2013).

For the photocard layer examined in this study, the average intensity of the Amide I peak measured at three different points is approximately the same of the average intensity of the cellulose peak at around 1100 cm^{-1} measured at the same three points. The small difference between these two values is consistent with the pattern reported in previous studies. Considering the approximate date of these prints, around the 1850s, and assuming that the binder is albumen, the results are consistent with the use of **a single-coated albumen layer**.

In the ATR-FTIR spectra collected from three different points on the brown support, a relatively weak peak was observed at around 1642 cm^{-1}, together with a shoulder on its right side. Previous studies have linked the presence of these two low-intensity bands to gelatin sizing added to the paper during manufacture. These bands are generally assigned to Amide I and Amide II, which are characteristic of protein-based materials such as gelatin. In contrast, the ATR-FTIR spectra collected from three points on the white support showed almost no clear signal in the Amide II region, unlike the brown support. Only a weak peak around 1640 cm^{-1} was observed, which may be related to the H–O–H bending vibration of absorbed water in the paper structure.

To confirm and complement the information obtained about the binders, ER-FTIR measurements were carried out on additional areas of the photograph. The results obtained from the photocard layer were generally similar to those from ATR-FTIR. However, in the ER-FTIR spectra, the cellulose bands were partly masked by the protein-related amide bands and were therefore less clearly distinguished.

In ER-FTIR, the way infrared light is reflected from the sample depends strongly on the surface texture. Smoother surfaces tend to produce more regular, mirror-like reflection, whereas rougher surfaces scatter the light more strongly. The amount of reflected light at each wavelength also

depends on the optical properties of the material, such as absorption and refractive index, which can cause some changes or distortion in the shape of the spectrum. Previous studies have shown that, because of the glossy surface of albumen prints, the image layer can dominate the ER-FTIR spectrum. In addition, the presence of combination bands in the 2250–1870 cm^{-1} region of the ER-FTIR spectrum can indicate the presence of barium sulfate ($BaSO_4$), or a baryta layer, which is associated with gelatin prints (Freixas-Jambert et al. 2024). However, these bands were not present in the spectrum of the sample, and this is consistent with the lack of the Ba emission in the pXRF measurements. Therefore, the absence of this spectral feature provides less support for identifying the photograph as a gelatin print.

The ER-FTIR analysis of the brown support, unlike the ATR-FTIR results, did not show a clear Amide II peak that could confirm strongly the presence of protein-based sizing in the paper. Only a peak around 1640 cm^{-1} was observed, so the presence of gelatin sizing in the brown support is still under question.

A comparison between the ER-FTIR spectrum of the brown support and that of a modern paper sample showed a high degree of similarity in their overall spectral profiles, including the presence of the peak around 1640 cm^{-1}. However, two differences were observed at around 1794 and 872 cm^{-1}, where peaks appeared in the modern paper but were absent from the brown support. Since ER-FTIR has not been extensively applied to the study of cellulose-based materials, the exact origin of these differences remains unclear. Nevertheless, the sharp 1794 cm^{-1} peak may be related to calcium carbonate ($CaCO_3$), which is commonly added to modern paper to increase whiteness and reduce acidity. A particularly interesting result came from comparing a foxed area with an unfoxed area on the same brown support. In the foxed area, an additional peak around 1570 cm^{-1} was clearly visible, while this peak was absent from the unfoxed area. Since foxing is a broad and complex topic and falls outside the scope of this study, the origin and significance of this spectral difference could be investigated further in future research.

At this stage, based on the results obtained from the different analytical techniques, the evidence is more consistent with an albumen print rather than a gelatin print. Finally, XRF analysis was carried out to investigate the elemental composition of the sample and identify the elements present on the surface of the photograph. The XRF measurements obtained from the darkened (Dmax) and clear (Dmin) areas of the photocard did not show any significant differences. However, a higher

intensity of elements such as silver (Ag) would have been expected in the darker areas of the image. This lack of variation may be related to the severe fading of the photograph over more than 170 years, which likely resulted in the reduction or loss of a significant amount of the image-forming silver. However, the Ag Kα peak around 22 keV is detected with sufficient intensity above background (Fig. 35), and it is sufficient for the detection of the element. Moreover, the silver signal associated with the Ag Lα peak at approximately 2.98 keV is also slightly stronger in the photo layer than in the supporting paper (Fig. 36), although the quantification remains uncertain due to the severe overlap with the argon peak originating from the air excitation.

Based on the comparison of the peak intensities obtained, iron and calcium showed the strongest signals across all three layers. The main peaks associated with these elements were Fe Kα at approximately 6.40 keV and Ca Kα at approximately 3.69 keV. The higher intensity of these elements was particularly evident in the brown support layer, which may be related to the darker color of this layer and the possible presence of a higher amount of iron-containing compounds. The strong Fe signal detected in the photocard layer may also be partly attributed to the penetration depth of XRF, allowing signals from elements present in the underlying support layers to be detected (Liu 2024). Although iron (Fe) has been reported in previous XRF studies of albumen prints (Modica et al. 2017), it cannot be considered a specific marker for identifying the albumen process, as its presence may originate from the paper support, fillers, impurities, or other components present in historical photographs.

Sulfur (S) was another element that showed a higher signal intensity in the photocard layer compared with the other two layers. However, the interpretation of its presence can lead to different conclusions. If a gelatin-based process is considered, the presence of sulfur in the photocard layer could be associated with the baryta layer commonly found in gelatin prints. However, due to the absence of strong and characteristic peaks of baryta-related elements, such as barium (Ba) and strontium (Sr), this hypothesis cannot currently be confirmed.

On the other hand, a significant amount of sulfur is naturally present in egg white. Therefore, the presence of sulfur in the photocard layer can also be consistent with the presence of an albumen-based binder. In general, albumen contains approximately 0.195% sulfur, and about 29.85% of the total sulfur content originates from its main protein component, ovalbumin. Among the amino acids that make up this protein, cysteine and methionine are two sulfur-containing amino acids of

particular importance. In cysteine, the sulfur atom is part of a chemical group known as a sulfhydryl or thiol group (R–SH). Two cysteine molecules can become connected through an oxidation reaction, forming a disulfide bond (R–S–S–R). These disulfide bonds act as internal connections within the protein structure. By linking different parts of the protein chain, they help maintain the three-dimensional structure and stability of the protein. In other words, these bonds play an important role in preserving the natural spatial structure of albumen proteins. In contrast, methionine also contains sulfur, but this sulfur is present in a different chemical structure (R-S-CH3). The sulfur in methionine can also participate in chemical reactions, particularly oxidation reaction (Messier 1991). In the case of albumen prints, sulfur can react with silver and contribute to image fading and loss of detail, this probably happened in the investigated photograph sample (Reilly et al. 1982; Messier 1991). Hence, the increased sulfur signal may also suggest the presence of sulfur-containing degradation compounds formed from the albumen binder (Puškárová 2016).

The other elements detected in the XRF spectra were mainly associated with the paper support and its fillers. The presence of gold, which is considered one of the characteristic elements of toning treatments commonly applied to albumen prints, was not confirmed.

For a more accurate identification of several elements and to improve the quality of XRF data, a helium flux system could be applied to the measurements. This approach reduces the emission signal by air molecules, thereby improving the detection of all peaks overlapping with argon.

Considering all the evidence obtained, including the date of the photograph and the photographic processes commonly used during that period, the possibility that this image was produced using the gelatin silver print process is considered highly unlikely. This technique became widely adopted mainly in the late nineteenth century, and photographic papers with a baryta layer were introduced in 1866 (Zamboni et al. 2021). Among the two earlier processes, salt print and albumen print, the clear presence of the Amide I and Amide II bands in the photocard layer, together with the presence of detectable silver and the high intensity of the sulfur signal in this layer compared with the other two layers, clearly supports the likelihood of an albumen-based process.

Furthermore, the observed deterioration patterns are consistent with the known aging behavior of albumen prints. Previous aging studies have shown that exposure to air, heat, and moisture can lead to characteristic degradation phenomena in albumen prints, including yellowing of highlights, loss of fine image details, overall fading of the image, and changes in image color (Reilly et al. 1982).

Considering the approximate date of production, the stronger signals associated with a protein-based binder compared with those related to cellulose, and the consistency of the observed deterioration features with albumen prints, the photograph was most likely produced using the albumen print technique, probably in the form of a single-coated albumen print.

4.2 Conclusions

The present study focused on a historical portrait photograph dating approximately to 1850–1855, attributed to the German photographer and lithographer Friedrich Carl Vogel. The photograph was investigated using a combination of non-invasive analytical techniques, including optical and confocal laser microscopy, ATR-FTIR, Micro-FTIR, and XRF.

One of the main challenges of this study was the inability to take a sample from the photocard layer. Techniques such as gas chromatography could have provided more precise information about the type of protein present in this layer. However, even the smallest sample would have caused irreversible damage to the extremely thin surface of the photocard layer. Moreover, since this layer covers only the circular image area, sampling the other layers would not have provided sufficient information to compensate for the lack of a sample from the photocard itself.

Consequently, the data obtained in this study represent the maximum amount of information that could be obtained through non-invasive techniques without causing damage to the object. Nonetheless the analytical results, considered alongside macroscopic observations, previous studies, and historical documentation are sufficient to interpret the photographic process adopted, and strongly support the hypothesis that the photograph was produced using the albumen printing process, with the albumen likely applied as a single, thin layer.

The weak load of the sensitive layer caused a poorly contrasted original image, that had to be manually retouched in several parts. Further, the extensive deterioration that the photograph has undergone over time, including widespread foxing, yellowing, and severe fading, has left the subject's facial features severely compromised. These changes have further complicated the identification of the photographic process used approximately 170 years ago.

References

Ardelean E. and Melniciuc-Puică N. 2013. "Conservation of Paper Documents Damaged by Foxing." *European Journal of Science and Theology* 9 (2): 117–124. https://www.ejst.tuiasi.ro/Files/37/11_ArdeleanMelniciuc.pdf

Artioli G. 2010. *Scientific Methods and Cultural Heritage: An Introduction to the Application of Materials Science to Archaeometry and Conservation Science*. Oxford: Oxford University Press

Barro, L., Sanderson, K., Centeno, S. A. and Saunders, B. 2020. "The Exhibition and Characterization of Seven Salted Paper Prints." *Journal of the American Institute for Conservation*. doi:10.1080/01971360.2019.1696914

Baruzzo E. 2020. "Zinelli, Federico Maria." Dizionario Biografico degli Italiani, vol. 100. Treccani. https://www.treccani.it/enciclopedia/federico-maria-zinelli_(Dizionario-Biografico/).

Cain, C. E. and Miller, B. A. 1984. 'Proposed classification of foxing', *Book and Paper Group Annual*, 3, pp. 29–30. https://cool.culturalheritage.org/coolaic/sg/bpg/annual/v01/bpga01-06.pdf

Clarke G. 1997. *The Photograph.* Oxford: Oxford University Press.

Derrick M. R., Stulik D. and Landry J. M. 2000. *Infrared Spectroscopy in Conservation Science*. Los Angeles: Getty Publications

Elliott A. D. 2020. Confocal Microscopy: Principles and Modern Practices. *Current Protocols in Cytometry* 92(1): e68. Doi: 10.1002/cpcy.68

Figueira, F., Matos, M., Nunes, A., Afonso, M., Rocha, A. C., Campelo, J., and Ferreira, T. 2020. “Considerations about foxing stains in three paper collections ranging from the 16th to the 20th century.” *Conservar Património* 35: 45–57. https://doi.org/10.14568/cp2019022

Freixas-Jambert, R., Ruiz-Recasens, C., Nieto-Villena, A., and Oriola-Folch, M. 2024. “Non-Invasive Characterisation of Bromoil Prints by External Reflection FTIR Spectroscopy.” *Molecules* 29: 5833. https://doi.org/10.3390/molecules29245833.

Garside, P., and Wyeth, P. 2003. “Identification of Cellulosic Fibres by FTIR Spectroscopy: Thread and Single Fibre Analysis by Attenuated Total Reflectance.” *Studies in Conservation* 48(4): 269–275. https://www.jstor.org/stable/1506916?seq=1

Geminiani, L., Campione, F. P., Corti, C., Giussani, B., Gorla, G., Luraschi, M., Recchia, S., & Rampazzi, L. (2025). *Non-invasive identification of historical textiles and leather by means of external reflection FTIR spectroscopy*. Spectrochimica Acta Part A: Molecular and Biomolecular Spectroscopy, 326, 125184. https://doi.org/10.1016/j.saa.2024.125184

Guerrero, A. and Silva, J. (2023) ‘Caracterización de materiales en fotografías a la albúmina del álbum de memorias de Calouste Sarkis Gulbenkian’, *Conservar Património*. doi: 10.14568/cp26220.

Hill, G. (2018) *Caring for photographic materials*. Ottawa: Canadian Conservation Institute, Government of Canada. Available at: https://www.canada.ca/en/conservation-institute/services/preventive-conservation/guidelines-collections/photographic-materials.html (Accessed: 27 August 2026).

Hirsch R. 2024. *Seizing the Light: A Social & Aesthetic History of Photography*. New York: Routledge

International Center of Photography. 1984. Encyclopedia of Photography. New York: Crown Publishers.

Kaur H., Rana B., Tomar D., Kaur S., and Jena K. C. 2021. “Fundamentals of ATR-FTIR Spectroscopy and Its Role for Probing In-Situ Molecular-Level Interactions.” In *Modern Techniques of Spectroscopy*, edited by D. K. Singh et al. Springer Nature Singapore. https://doi.org/10.1007/978-981-33-6084-6_1

Krstić D., Pavec M., and Schauperl Z. 2013. “Characterization of Foxing Stains in Eighteenth Century Books.” *HDKBR INFO Magazin* 3 (3): 32–39. https://hrcak.srce.hr/file/219010

Lavédrine B. 2009. *Photograph of the past: process and preservation*. Los Angeles: Getty Publications.

Lavédrine B. 2003. *A Guide to Preventive Conservation of Photograph Collections*. Los Angeles: Getty Publications.

Liu, G.-L., Chen, T.-C. and Kazarian, S.G. (2024) ‘Identification of black and white antique photographs via non-destructive microscopic and spectroscopic techniques coupled with chemometric approaches’, *Microchemical Journal*, 200, 110297. doi: 10.1016/j.microc.2024.110297.

Messier, P. (1991) ‘Protein chemistry of albumen photographs’, *Topics in Photographic Preservation*, 4, pp. 124–135

Modica, A., Alberghina, M.F., Brai, M., Bruno, M., Di Bella, M., Fontana, D. and Tranchina, L. (2017) ‘XRF analysis to identify historical photographic processes: The case of some Interguglielmi Jr.’s images from the Palermo Municipal Archive’, *Radiation Physics and Chemistry*, 135, pp. 76–80. doi: 10.1016/j.radphyschem.2017.02.026

Nieto-Villena A., Martínez Mendoza J. R., Ramírez-Saito M. Á., Arauz-Lara J. L., de la Cruz-Mendoza J. Á., Lobo Guerrero-Serrano A., Ortega-Zarzosa G., and Solbes-García Á. 2019. *Exploring confocal microscopy to analyze ancient photography*. Journal of Cultural Heritage 36: 191–199. https://doi.org/10.1016/j.culher.2018.07.014.

Nodari, L., and Ricciardi, P. 2019. "Non-invasive identification of paint binders in illuminated manuscripts by ER-FTIR spectroscopy: A systematic study of the influence of different pigments on the binders' characteristic spectral features." *Heritage Science* 7: 7. https://doi.org/10.1186/s40494-019-0249-y.

Oravec M., Haberová K., Jančovičová V., Machatová Z., Čeppan M., and Huck C. W. 2019. Identification of the historic photographic print materials using portable NIR and PCA. Microchemical Journal 150: 104202. https://doi.org/10.1016/j.microc.2019.104202

Paladini, G., Venuti, V., Crupi, V., Majolino, D., Fiorati, A., and Punta, C. 2020. "FTIR-ATR Analysis of the H-Bond Network of Water in Branched Polyethyleneimine/TEMPO-Oxidized Cellulose Nanofiber Xerogels." *Cellulose* 27: 8605–8618. https://doi.org/10.1007/s10570-020-03380-7.

Peres M. R. (ed.). 2007. Focal Encyclopedia of Photography: Digital Imaging, Theory and Applications, History, and Science. Burlington, MA: Focal Press.

Poggialini, F., Campanella, B., Giostrella, C., Lorenzetti, G., Palleschi, V., Raneri, S. and Legnaioli, S. (2025) 'Non-Invasive Investigation of 19th-Century Photographs: Enrico Van Lint's Historical Collection in Pisa', *Heritage*, 8, 59. doi: 10.3390/heritage8020059.

Puškárová, A., Bučková, M., Habalová, B., Kraková, L., Maková, A. and Pangallo, D. (2016) 'Microbial communities affecting albumen photography heritage: a methodological survey', *Scientific Reports*, 6, 20810. doi: 10.1038/srep20810.

Reilly J. M. 1980. *The Albumen & Salted Paper Book: The History and Practice of Photographic Printing*, 1840–1895. Rochester, New York: Light Impressions Corporation. https://cool.culturalheritage.org/albumen/library/monographs/reilly/albumen-reilly_delivery.pdf

Ricci C., Bloxham S. and Kazarian S. G. 2007. "ATR-FTIR Imaging of Albumen Photographic Prints." *Journal of Cultural Heritage* 8(4): 387–395. https://doi.org/10.1016/j.culher.2007.07.002.

Seminario Vescovile della Diocesi di Treviso. 2020. "*Archivio fotografico*." Accessed August 25, 2026. https://www.diocesitv.it/seminariotreviso/archiviofotografico/

Stemp W. J., Lerner H. J., and Kristant E. H. 2018. *Testing Area-Scale Fractal Complexity (Asfc) and Laser Scanning Confocal Microscopy (LSCM) to Document and Discriminate Microwear on Experimental Quartzite Scrapers*. Archaeometry 60 (4): 660–677. https://doi.org/10.1111/arcm.12335.

Stulik D. C. and Kaplan A. 2013. *The Atlas of Analytical Signatures of Photographic Processes: Salt Print*. Los Angeles: The Getty Conservation Institute.

Stulik, D. C. and Kaplan, A. 2013. *The Atlas of Analytical Signatures of Photographic Processes: Albumen*. Los Angeles: The Getty Conservation Institute.

Stulik D. C. and Kaplan A. 2013. *The Atlas of Analytical Signatures of Photographic Processes: Silver gelatin*. Los Angeles: The Getty Conservation Institute

Talbot Correspondence Project. 2026. "Talbot's Correspondence: Search the Letters." Accessed August 26, 2026. https://foxtalbot.dmu.ac.uk/letters/transcriptFreetext.php

Taylor R. and Ware M. 2003. “Pilgrims of the Sun: The Chemical Evolution of the Calotype 1840–1852.” *History of Photography* 27(4): 308–319 .https://doi.org/10.1080/03087298.2003.10441266.

Tsantiri, K., Kokla, V. and Karabotsos, A. (2024) ‘Study of Toned Photographs of the Late 19th and Early 20th Century Using Multispectral Imaging and SEM/EDS Analysis’, *Restaurierung: Zeitschrift für Restaurierung, Denkmalpflege und Museumstechnik*, 45(4), pp. 277–295. doi: 10.1515/res-2024-0015

Wagner, S., Clarke, M. L., & Walker, J. M. (2020). “Linnaeus Tripe and Lightly Albumenized Prints in the 1850s: Characterization, Analysis and Process Identification.” *Journal of the American Institute for Conservation, 59*(3–4), 218–234. https://doi.org/10.1080/01971360.2019.1609824

Walker, J. M., and Berrie, B. H. 2023. “Influence of Image Density and Interfacial Surfaces on ER-FTIR Spectra of 19th Century Photographic Print Processes.” *Journal of Cultural Heritage* 63: 1–10. https://doi.org/10.1016/j.culher.2023.07.007.

Wikipedia. 2026. “Photographic Print Toning.” Accessed August 25, 2026. https://en.wikipedia.org/wiki/Photographic_print_toning.

Zamboni, C.B., Redígolo, M.M., Miura, V.T., et al. (2021) ‘Non-destructive analysis in the study of historical photographs by pXRF and ATR-FTIR spectroscopies’, *Journal of Forensic Sciences*, 66, pp. 1048–1055. doi: 10.1111/1556-4029.14680

Zotti, M., Ferroni, A. and Calvini, P. (2011) ‘Mycological and FTIR analysis of biotic foxing on paper substrates’, *International Biodeterioration & Biodegradation*, 65, pp. 569–578. doi: 10.1016/j.ibiod.2010.01.011.

Thesis

Pellegrina M. 2024. *The Egyptian blue pigment: identification, manufacturing techniques, provenance*. Master's thesis. Università degli Studi di Padova. https://hdl.handle.net/20.500.12608/70316

Taati Anbuhi F. 2024. *Pigments identification from Romanino's frescoes in the Duomo Vecchio, Brescia*. Master's thesis. Università degli Studi di Padova. https://hdl.handle.net/20.500.12608/78745

Database of IR and Raman spectroscopy

http://www.irug.org/